UNIVERSITA' DEGLI STUDI MILANO - BICOCCA
Scuola di Dottorato in Scienze Mediche Sperimentali e Cliniche
Dottorato in Tecnologie Biomediche
Ciclo XXIII

Quantification methods for PET/CT oncological studies and correlation approaches with proteomic and hystological data.

Tutor interno: Prof.ssa Cristina MESSA
Tutor esterno: Prof.ssa Maria Carla GILARDI
Tutor esterno: Dott.ssa Isabella CASTIGLIONI

Tesi di Dottorato di:
Francesca GALLIVANONE
Matricola 716438

ANNO ACCADEMICO 2009/2010

A mio figlio Duecento
per avermi fatto sognare la maternità
A mio figlio Samuele
per avermene regalato il dono

Contents

Abstract

The integration of molecular medicine data is one of the more ambitious challenges of the "personalized medicine". Recent studies [1, 2, 3] have demonstrated that some *in vivo* parameters correlate systematically with information obtained from *ex vivo* proteogenomic analysis, opening a new role of *in vivo* molecular imaging in the current approach of integrated molecular medicine. Data integration requires the development of new methods and infrastructures for the correct and efficient use of data, from their collection and archiving, to their combined analysis, with the purpose to extract new knowledge.

Aim of the PhD thesis was the development and validation of methods for the extraction of quantitative biomarkers from *in vivo* molecular imaging (from PET/CT oncological studies) to be correlated with *ex vivo* molecular imaging indexes (from hystological and proteomic data).

The first part of this work was dedicated to the assessment and the development of methods, as well as to the implementation of software tools, for qualitative and quantitative analysis of PET/CT oncological studies.

Analysis of signal elaboration and visualization from PET/CT images was performed: images were exported from hospital (Scientific Institute San Raffaele, Milan, Italy) RIS-PACS archive, algorithms for image visualization in transaxial, sagittal and coronal projection were tuned and smoothing filters were implemented. In order to integrate functional data from PET images with morphological data from CT images, methods for fusion of PET and CT images were developed.

As result of this part of the PhD work, a new software tool was developed and implemented: cOuch (Correlative and Collaborative Touch System) performs collaborative qualitative and quantitative analysis of PET/CT studies with accurate correction for physical effects inducing errors in quantification of radioactivity concentration (Partial Volume Effect). The software was developed in MATLAB R2008a and was implemented on a touchscreen hardware system, in order to optimize image management and visualization as well as to improve quantitative analysis.

Algorithms for the identification and radioactivity measurement on a region of interest (ROI) on PET/CT images were developed following approaches already proposed [4]. Different kinds of ROIs were developed: manually drawn irregular ROI, circular ROI interactively drawn by the operator selecting center and radius, thresholded ROI automatically defined, requiring as input maximum intensity pixel as well as ROI neighborhood.

ROI quantitative data (mean and maximum radioactivity concentration, ROI activity, volume, Standardized Uptake Value (SUV)) were obtained by interpolation of contour pixels: SUV was chosen as the quantitative biomarker to consider.

Obtained quantitative data are affected by PVE [4]: a PVE correction method, based on Recovery Coefficient (RC) was developed. RC coefficients were obtained by experimetal measurements with a standard phantom simulating oncological whle-body lesions (NEMA IQ phantom [5]).

Six different techniques were evaluated to measure sphere radioactivity concentration (C_m) and sphere diameter d_m on PET/CT images:

- Operator Dependent Technique using maximum value of radioactivity concentration - OD_{max}: C_m is obtained as the maximum value of radioactivity concentration in a manually drawn

ROI on PET image ($OD_{max-PET}$) or on CT image and then copied on PET image (OD_{max-CT}). d_m value is obtained as sphere-equivalent diameter from the manually drawn ROI.

- Operator Dependent Technique using the mean value of radioactivity concentration (manually drawn ROI) - OD_{man}: C_m is obtained as the mean value of radioactivity concentration in a manually drawn ROI on PET image ($OD_{mean-PET}$) or on CT image and then copied on PET image ($OD_{mean-CT}$).d_m is measured as sphere-equivalent diameter from the manually drawn ROI.

- Operator Independent Technique (thresholded ROI) - $OI_{threshold}$: C_m is the maximum (OI_{max}) or the mean value (OI_{mean}) of radioactivity concentration in a ROI drawn on PET image using an isocontour at a fixed threshold (from 40% to 70%) from the maximum value; d_m is obtained as sphere-equivalent diameter of this ROI.

The background radioactivity concentration was considered free by errors and it was measured as mean of radioactivity concentration of 20 ROIs drawn on the background.

RC coefficients were calculated as the ratio between measured (S/B_m) and actual (S/B_{GS}) sphere-to-background ratio for each of the six considered measurement technique; RC values obtained for the same S/B_m and for different diameters were fitted with a three-parameter hyperbolic function: six set of RC curves for each measurement techniques were obtained at different S/B_m intervals as a function of d_m and were used for the PVE correction. A proper tool was implemented in the cOuch software for the PVE correction with the developed method.

The validation of the PVE correction method, using each measurement technique was performed using three different anthropomorphic phantoms simulation body regions (thorax, breast and brain) filled with spheres of different diameter simulating oncological lesions.

Clinical feasibility was evaluated on a group of patients, considering the applicability and the consistency of the PVE correction method. Two groups of patients were considered. The first group consisted of sixteen oncological patients with different pathologies that underwent two PET/CT exams (a basal and a follow up study): the effect of the PVE correction on SUV changes due to the therapy was evaluated. The second group consisted of twelve breast cancer patients that underwent a PET/CT exam before surgery: the effect of PVE correction on the absolute value of SUV was evaluated.

The second part of this work was devoted to the assessment and the development of procedures for the correlation of the extracted PET/CT quantitative biomarker and histopathological and proteomic indexes.

A protocol started involving patients with breast cancer that needed a surgery procedure. The protocol consisted of a PET/CT exam performed before surgery; after the surgical procedure, the surgical species were analyzed by the pathologist and sent to the lab for proteomic analysis, in order to evaluate protein expression.

Storing and saving of the patient data was optimized so that the procedure was effective, fast and easy to perform for all the involved specialists (surgeon, nuclear physician, pathologist and biologist): a virtual lab connecting all the involved unit was developed, as optimal model for the management of integrated protocols for single-patient data collection focused to prognosis, diagnosis, and monitoring of treatment response.

An analysis of methods to integrate and correlate *in vivo* and *ex vivo* molecular imaging biomarkers was performed. In the cOuch software, two different tests (Mann-Whitney test and Kruskal-Wallis test) were implemented to study the correlations between the quantitative PET/CT parameter and proteomic or hystopathological data. Methods for the multiple correlation between *in vivo* and *ex vivo* molecular imaging data were also studied.

The implemented infrastructure was tested for conflicts in data submission, recovery and data loss or corruption, and the efficiency of statistical analysis was evaluated on a set of simulated correlated data.

Sommario

L'integrazione dei dati di medicina molecolare è oggi una delle più ambiziose sfide della medicina personalizzata. Studi recenti [1, 2, 3] hanno dimostrato che alcuni parametri ottenuti *in vivo* correlano sistematicamente con informazioni di proteogenomica ottenute dunque da analisi *ex vivo*: queste scoperte aprono ad un nuovo ruolo delle metodiche di *imaging* molecolare *in vivo* in un nuovo approccio di medicina molecolare integrata.

L'integrazione tra dati *in vivo* ed *ex vivo* richiede lo sviluppo di nuovi metodi ed infrastrutture per un uso efficiente e corretto dei dati e per la raccolta ed il salvataggio dei dati stessi, così da poterne effettuare un'analisi combinata che permetta di ottenere nuovi ed interessanti risultati.

Scopo di questo lavoro di tesi è stato lo sviluppo e la validazione di metodi per l'estrazione di biomarker quantitativi da studi oncologici di imaging molecolare *in vivo* PET/CT da correlare con indici di imaging molecolare *ex vivo* (dati di istologia e proteogenomica).

La prima parte del lavoro è stata dedicata alla valutazione e allo sviluppo di un metodo, oltrechè all'implementazione di un software dedicato, per l'analisi qualitativa e quantitativa di studi oncologici PET/CT.

Sono state approfondire problematiche legate alla lettura, visualizzazione ed elaborazione del segnale immagine digitale: le immagini sono state esportate dal sistema di archivio RIS-PACS dell'ospedale (IRCCS San Raffaele), sono stati messi a punto algoritmi per la lettura e visualizzazione delle immagini PET e CT nelle proiezioni transassiali, coronali e sagittali e infine sono stati studiati e implementati filtri in grado di ridurre l'effetto di granulosità dell'immagine. Sono stati implementati metodi per la fusione delle immagini PET e TC ottenendo l'integrazione dell'informazione funzionale PET con l'informazione anatomica TC.

Prodotto di questa prima fase e' stato lo sviluppo e l'implementazione di un software dedicato: Couch (Correlative and Collaborative Touch System) è pensato per analisi collaborative qualitative e quantitative di immagini PET/CT con un'accurata correzione per gli effetti fisici che inducono errori nella quantificazionde della concentrazione di radioattività (Effetto di Volume Parziale, PVE). Il software è stato scritto in MATLAB R2008a ed è stato implementato su un hardware touchscreen, per una migliore visualizzazione e gestione delle immagini PET/CT oltrechè per un'ottimizzazione delle procedure di analisi quantitativa.

Sono stati implementati algoritmi per il riconoscimento e il calcolo dell'attività in regioni di interesse (ROI) disegnabili sull'immagine PET oppure disegnabili sull'immagine TC e riportate successivamente sull'immagine PET, scegliendo di implementare diversi tipi di ROI sulla base di approcci già pubblicati in letteratura [4]: ROI di tipo irregolare, manualmente tracciabili dell'operatore e ottimizzate grazie al sistema hardwere touchscreen, ROI circolari, ottenute selezionando e variando interattivamente centro e raggio tramite un input manuale o da penna, ROI definite con un isocontorno a diverse soglie (dal 40% al 70%) dell'intensità massima del segnale, automaticamente definite a partire da un input (manuale o da penna) dell'operatore che fissa il pixel di intensità massima e l'intorno per il calcolo dell'isocontorno a soglia.

I valori quantitativi all'interno delle ROI (concentrazione di attività massima e media, attività, area e volume, *Standard Uptake Value* (SUV) [6] medio o massimo) sono ricavati tramite inter-

polazioni nei pixel di contorno: il valore di SUV è stato scelto come biomarker quantitativo da considerare.

I dati quantitativi così ottenuti sono soggetti a Effetto di Volume Parziale (PVE) [4]: è stato studiato ed implementato un metodo di correzione basato sull'uso di Coefficienti di Recupero (RC). Tali coefficienti sono stati ricavati con misure sperimentali usando un fantoccio standard per la Qualità dell'Immagine (NEMA IQ phantom) [5].

Sono state sviluppate sei tecniche per ricavare i valori della concentrazione di attività (C_m) e del diametro misurato d_m sull'immagine PET/CT:

- Tecnica Operatore Dipendente con l'uso del valore massimo di concentrazione - OD_{max}: C_m è ottenuta come il valore massimo della concentrazione di attività in una ROI disegnata manualmente sull'immagine PET ($OD_{max-PET}$) oppure sull'immagine TC e riportata successivamente sull'immagine PET (OD_{max-CT}). Il valore di d_m si ricava come diametro sfera-equivalente per la ROI disegnata.

- Tecnica Operatore Dipendente con l'uso del valore medio di concentrazione (ROI manuale) - OD_{mean}: C_m si ottiene come media in una ROI disegnata manualmente dall'operatore sull'immagine PET ($OD_{mean-PET}$) oppure sull'immagine TC e riportata poi sull'immagine PET ($OD_{mean-CT}$). Il valore di d_m è ricavato come diametro sfera-equivalente per la ROI disegnata.

- Tecnica Operatore Indipendente (ROI a soglia) - $OI_{threshold}$: C_m si ottiene come il valore massimo (OI_{max}) oppure come il valore medio (OI_{mean}) in una ROI a soglia (isocontorno dal 40% al 70%) disegnata sull'immagine PET, mentre il valore di d_m è ricavato come diametro sfera-equivalente per la ROI disegnata.

Il valore della concentrazione di attività nel fondo, considerato non influenzato da PVE, è stato misurato come media della concentrazione valutata in 20 ROI sul fondo.

I coefficienti RC sono stati calcolatati con rapporto tra il valore misurato (S/B_m) ed il valore vero (S/B_{GS}) del rapporo sfere-su-fondo ricavato per ognuna delle sei tecniche: i coefficienti RC ricavati sperimentalmente per sfere di diverso diametro ad uno stesso S/B_m sono stati fittati in funzione di d_m con una funzione iperbolica a tre parametri, ottenendo sei differenti set curve, uno per tecnica, a diversi intervalli S/B_m, che vengono utilizzate per la correzione per PVE.

E' stato implementato, all'interno di Couch, un appropriato tool dedicato alla correzione per PVE con il metodo sviluppato.

E' stata effettuata una validazione del metodo di correzione per PVE, usando tre diversi fantocci antropomorfi, che simulassero parti del corpo (torace, mammella, cervello), al cui interno sono state messe delle sfere simulanti lesioni oncologiche. E'stata ricavata l'accuratezza del metodo di correzione con le diverse tecniche di misura ed è stata fatto un confronto delle diverse accuratezze al fine di poterne valutare le caratteristiche in termini di vantaggi e svantaggi.

Una valutazione dell'uso clinico del metodo di quantificazione con correzione per PVE è stata effettuata su un insieme di pazienti, osservando anche l'applicabilità e la consistenza del metodo. Sono stati scelti e seguiti due gruppi di pazienti. Il primo gruppo formato da sedici pazienti oncologici con diverse patologie che avessero effettuato due studi PET/CT successivi, uno studio basale e uno studio di follow up, così da analizzare l'effetto della correzione sulle modificazioni dell'SUV indotti dei trattamenti e terapie. Nel secondo gruppo sono state arruolate dodici pazienti con tumore al seno che hanno effettuato uno studio PET/CT precedente all'intervento chirurgico di asportazione della massa tumorale. Su tale gruppo è stato effettuato uno studio sull'effetto della correzione sul valore assoluto dell'SUV.

La seconda parte del lavoro è stata dedicata alla valutazione e allo sviluppo di procedure per la correlazione del parametro quantitativo PET/CT (SUV) con gli indici di istopatologia e di proteomica.

E' stato studiato e avviato un protocollo che coinvolge pazienti con carcinoma mammario: le pazienti arruolate e destinate all'intervento chirurgico hanno effettuato un esame PET/CT nei giorni precedenti l'intervento, la parte asportata chirurgicamente è stata analizzata dall'anatomopatologo, per le analisi di routine, lasciando una piccola parte del pezzo per l'analisi proteomica, al fine di poter valutare le proteine sovra- o sotto- espresse nel tessuto mammario canceroso rispetto a quelle presenti nel tessuto sano.

E' stato affrontato il problema della raccolta e del salvataggio dei dati delle pazienti in modo che questa procedura fosse efficace e rapida, per tutte le figure professionali coinvolte dal protocollo. E' stato messo a punto un laboratorio virtuale, gestito via web, per facilitare la raccolta dei dati da tutte le unità coinvolte. E' stata sviluppata dunque una infrastruttura dedicata, che unisce tramite internet diversi ambulatori, reparti diagnostici, clinici ed ospedalieri e laboratori di ricerca, rappresentando un modello di infrastruttura ottimale per la gestione di progetti di medicina integrata, con la condivisione di grandi database di dati diversi.

Sono stati quindi affrontati gli aspetti metodologici legati all'integrazione dei dati di imaging molecolare *in vivo* ed *ex vivo*. Nel programma cOuch sono stati implementati due tipi di test (Mann-Whitney test e Kruskal-Wallis test) per studiare le correlazioni tra il parametro quantitativo PET/CT (SUV) e i parametri istopatologici o le proteine up- o down-regolate nel tessuto malato. Sono state quindi studiate metodologie per la ricerca di correlazioni multiple tra più parametri.

L'infrastruttura sviluppata è stata testata per evitare conflitti nella sottomissione e nella memorizzazione dei dati, per prevenire la perdita o la corruzione dei dati. E'stata infine valutata l'efficienza delle procedure statistiche usando un dataset di dati correlati, simulati *ad hoc*.

Chapter 1

Introduction

The Positron Emission Tomography (PET) is a functional imaging technique that uses a radiopharmaceutical, that is a chemical compound labeled with a radioactive isotope, to image body districts on the basis of the accumulation of the radioactive tracer. Using different kinds of radiopharmaceutical, a large variety of biological process can be imaged, such as glucose consumption, blood perfusion, hypoxia, protein expression or receptor concentration. Given the ability of PET to image biological process, this technique is widely used to detect and to observe physio-pathological processes of clinical relevance.

In this chapter a general overview of the physics process behind the PET signal, of the PET acquisition and image analysis, from a qualitative and a quantitative point of view, is presented. Some topics will be dedicated to physical phenomena that can disturb the PET signal, with a particular attention to the Partial Volume Effect. A brief explanation of the different technique to correct for PVE will be presented.

1.1 PET Physics and Instrumentation

1.1.1 β^+ decay

Between the unstable nuclides, also termed radionuclides, there are some radionuclides that are rich in protons. These radionuclides undergo a decay process in which a proton is converted into a neutron with the emission of a neutrino (ν) and a positron (β^+).The conversion process of the proton into a neutron can be represented as in (2.1)

$$p \rightarrow n + \beta^+ + \nu \tag{1.1}$$

Due to the energy conservation, the β^+ decay can only happen inside nuclei and the radionuclide has to have a transition energy of at least 1.022 MeV. The decay energy beyond 1.022MeV is converted into kinetic energy shared by the β^+ particle and the neutrino. Equation (1.2) represent a β^+ decay for a typical radionuclide:

$$^{18}_{9}F_9 \longrightarrow {}^{18}_{8}O_{10} + \beta^+ + \nu \tag{1.2}$$

After emission from the nucleus, the positron loses kinetic energy by interactions with the surrounding matter, then the positron combines with an electron when they both are essentially at rest, forming a metastable intermediate species called positronium. Positronium is a non-nuclear, hydrogen-like element composed of the positron and electron, it has a mean life of around 10^{-7} seconds, and decay with a subsequent annihilation of positron and electron with the conversion of

the particles into two photons at 511 keV energy, which are emitted, for the momentum conservation, in opposite directions. Positronium formation occurs with a high probability in gases and metals, but only in about one-third of cases in water or human tissue where direct annihilation of the electron and the positron is more favorable.

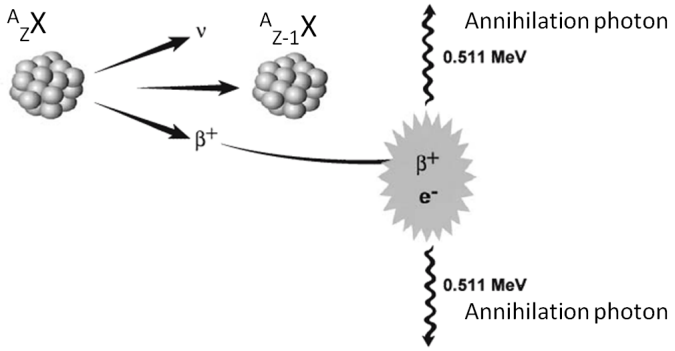

Figure 1.1: The β^+ decay

Figure 1.1 show the β^+ decay, schematically. Detection of the two opposite 511keV photons in coincidence by two detectors is the basis of PET.

1.1.2 PET detectors and detector configurations

PET signal is generated by the detection in coincidence of two photons at approximately 511 keV.

Tho photons are measured by two detector within an energy window centered at 511 keV and within an electronic time window that defines the event as a coincidence event. The event is spatially located along the straight line that connect the two detector, defined Line Of Response (LOR).

In acquiring the coincidence events, three steps are followed:

1. The line that connects a detector pair (LOR) defines the location of a coincident event
2. The detectors measure two photons within a coincidence window, defined from the coincidence resolving time of the system (τ)
3. The two photon are checked if they are within the energy window centered at 511 keV

Radiation detection in PET is performed using solid scintillation detectors coupled to photomultiplier matrices that make possible the most efficient detection of the annihilation events. These solid detectors transform the 511 keV photons into visible light and the light photons are converted to an electrical pulse by a photomultiplier tube (PMT). The signal is analyzed by a dedicated electronic chain, including a coincidence circuit. Figure 1.2 represents the detection process for an annihilation event.

There are different properties that an ideal PET detector has to have:

- A good Stopping Power for 511 keV photons: it is important to maximize the number of photons which interact and deposit energy in the detector in order to measure all the annihilation signal
- An high Light Output: the conversion process of interacting annihilation photons into light photons has to be efficient

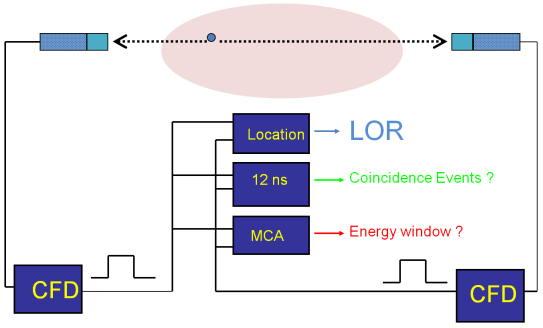

Figure 1.2: Detection of annihilation photons

- Fast response or short decay time: the scintillation decay time needed to convert the deposited energy into visible light has to be short in order to improve the detection efficiency at high count rate
- High Optical light transmission and no self absorption, so that each event of energy deposition is converted into electrical signal
- Index of refraction close to that of the PMT, so that the localization of deposition energy event is precise
- Low Cost

Between the different scintillator that have application in PET it can be found sodium iodide doped with thallium (NaI(Tl)), bismuth germanate $Bi_4Ge_3O_{12}$ (BGO), lutetium oxyorthosilicate doped with cerium Lu_2SiO_5:Ce (LSO), gadolinium oxyorthosilicate doped with cerium Gd_2SiO_5:Ce (GSO), and barium fluoride (BaF_2). Table 1.1 shows the properties of those different scintillators.

Table 1.1: Scintillation material used in PET systems and their properties

Property	NaI(Tl)	BGO	LSO	GSO	BaF_2
Effective atomic number (Z)	51	74	66	59	54
Density (g/cm^3)	3.7	7.1	7.4	6.7	4.9
Linear attenuation coefficient, μ(cm^{-1})	0.35	0.96	0.87	0.70	0.44
Scintillation decay time (ns)	230	300	40	60	0.6
Photon yield per keV	38	6	29	10	2
Light yield (%Na(Tl))	100	15	75	30	6
Fragile	Yes	No	No	No	Slight
Hydroscopic	Yes	No	No	No	No

Concerning the configuration and the arrangement of detectors in a PET scanner, we can found two main configurations:

- discrete, small-area detectors in rings or polygonal arrays completely encircling the patient
- continuous, large-area detectors requiring rotation of two or three detectors for complete angular sampling, or alternatively, arranged in a polygon (if flat) or in a circle (if curved) completely encircling the patient.

At the beginning PET detectors were arranged so that a single scintillation crystal was coupled to a single PMT. Subsequently, an arrangement with a large number of small detector elements spatially encoded using only four PMTs without a one-to-one coupling was developed in order to maximize the spatial resolution minimizing the cost of miniaturization of PMTs and associated electronics (block detector technology).

Pixelated detectors are an alternative to the block detector technology. In this case a matrix consisting of individual small-area detectors fixed onto a continuous light guide is coupled to a close-packed array of PMTs.

1.2 Data Acquisition

1.2.1 2D and 3D acquisition mode

In many PET systems, arranged in a multiring configuration, annular septa made of tungsten or lead are inserted between rings. In some scanners, septa are retractable or fixed, while in others, they are not incorporated. The presence or the use of this septa define the PET acquisition as a 2D or a 3D PET acquisition.

A 2D acquisition is performed using the septa. This configuration of the PET scanner allow to accept the coincidences stored between detector pairs on the same ring or, at least, between detectors of adjacent rings. In particular coincidences acquired between detectors on the same ring define the direct planes, while coincidences acquired between detectors in adjacent rings define cross planes (see Figure 1.3 a)).

In 3D acquisition, in absence of septa, the coincidences are acquired also between detectors placed in different rings (see Figure 1.3 b)).

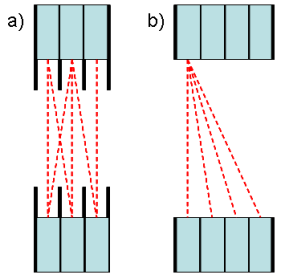

Figure 1.3: A schematic illustration of a 2D an 3D acquisition mode

The 2D acquisitions allow to reduce the scatter fraction (from 30-40% to 10-15%) while the sensitivity decreases due to the septa with respect to 3D acquisition where higher sensitivity improves signal-to-noise ratio [7].

PET/CT acquisitions

Positron Emission Tomography (PET), is a non-invasive molecular imaging technique that uses various radiolabeled compounds and visualizes metabolic differences between tissues. However in PET images most anatomic structures are poorly depicted, if not completely absent. As a consequence, it is difficult to localize tumor lesions precisely and, at the same times, the presence of some body regions showing a physiological uptake of radiotracer, makes difficult to interpret PET images when the neoplasm is located near an organ with physiological uptake. The importance

to correlate PET images with morphologically defined images leaded to the development of hybrid PET/CT systems, that combine a CT acquisition to a PET acquisition allowing to obtain PET images showing tissue metabolism co-registrated to CT images revealing tissue morphology.

Data acquisition in PET/CT is characterized by the acquisition of a CT scan followed by a PET scan. In a typical PET/CT protocol, with a static PET acquisition, the patient is injected with PET tracer and waits for 45 to 60 minutes for the uptake stabilization. After the waiting period, an initial scout scan like a conventional x-ray is obtained in order to define the axial extent of the body to be imaged. Then, the patient is moved to the CT field of view and a transmission CT scan is obtained for a period shorter than 1 minute. After the CT scan is completed, the patient is advanced inside the PET scanner.

The CT scan data are used both to calculate the attenuation corrections applied to PET images and to reconstruct the CT images. Reconstructed CT and PET images are then fused using appropriate algorithms.

PET/CT imaging eliminates the lengthy standard PET scans, with correction of an external source for attenuation correction, reducing the total scan time considerably and at the same time allow an efficient alignment and fusion of the CT (anatomical) and PET (functional) images, greatly improving the detection of lesions. Figure 1.4 show schematically the configuration of a PET/CT scanner.

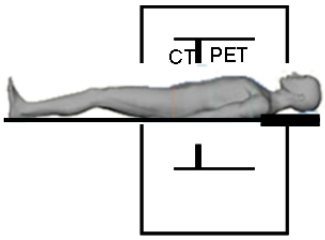

Figure 1.4: A schematic illustration of a PET/CT system

1.2.2 Data storage and Image Reconstruction

Detected coincidence events in PET are stored in a *sinograms*.

Consider an event of annihilation, as represented by the * symbol in Figure 1.5, and, for simplicity, consider a direct plane on a 2D acquisition mode.

On the same ring the coincidence event is detected by the two detector connected by the LOR represented by the red arrow. The considered LOR can be defined by the distance r from the center of the scan field and by the angle of orientation ϕ. The sinogram consists of a 2D matrix in which the distance r is represented on the x-axis and the angle ϕ on the y-axis: the coincidence event along the LOR (r, ϕ) will be assigned at the cross-point of r and ϕ values. A horizontal row at angle ϕ represents adjacent detector pairs that constitute parallel LORs at different r values, while a vertical raw represents all the LORs that are equally distant from the center of scan field.

It is clear that it is not known where, along the registered LOR, the event occurred and that many coincidence events arising from different locations along the LOR identified by a r value and a ϕ value are store in the same pixel, so the total counts in each pixel represent the number of coincidence events detected during the counting time along the LOR.

In case of 3D acquisition the sinogram has to take in account also the position of the detector pairs to different rings. Another coordinate is introduce as the co-polar angle ϑ that define the angular position of the LOR along the axial direction.

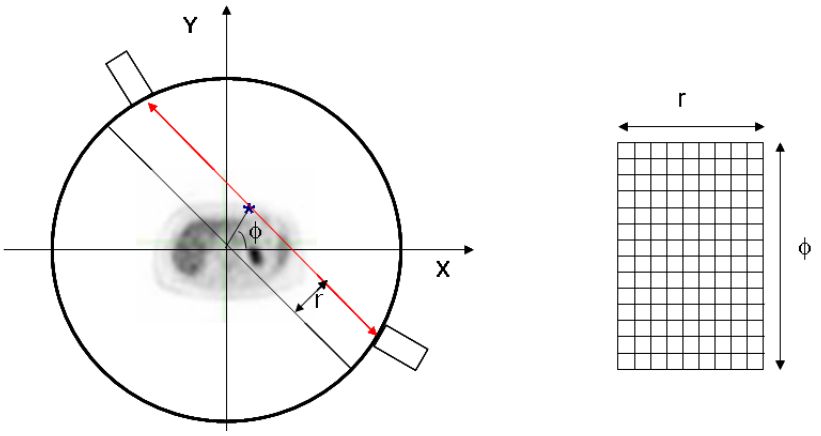

Figure 1.5: PET data acquisition in the form of a sinogram. Each LOR data is plotted in (r, ϕ) coordinates. Data for all r and ϕ values are plotted to yield sinogram

Data stored for all the registered sinograms, are processed to produce the images in the image reconstruction step.

Without excessive deepening, we can say that the are two groups of image reconstruction algorithms:

- Analytic algorithms: a linearity and shift invariant mathematical approach to data, where projection data in the sinograms are inverted without considering the presence of noise.
- Iterative algorithms: algorithms based on statistical estimation procedures such as maximum-likelihood (ML) and maximum a posteriori (MAP) estimation allowing a more accurate modeling of the data acquisition including physical phenomena involved in the process (detection, photon transport in tissues, the statistical distribution of the acquired data, i.e. the noise properties)

Iterative algorithms need a longer procession time with respect to analytic algorithms, but they allow a better noise characterization.

Filtered Back Projection is the more used analytic algorithm in PET system, while a very popular and fast iterative algorithm is the Ordered Subset Expectation Maximization (OSEM) algorithm.

1.2.3 Factors affecting acquired data

Random, scattered and spurious coincidences

The duty of PET detector is to measure the two photons at 511 keV generated by the annihilation process, named true coincidences (see Figure 1.6 a), but, in fact, some events that are registered from PET detectors, are not true annihilation events.

Figure 2.4 shows a schematic view of coincidence events sampled from PET detectors. In particular there are three kind of events that are incorrectly sampled as true coincidences:

- Random Coincidences occur if two annihilation photons generated from two separate decays are detected as true coincidences (see Figure 1.6 b). This phenomenon occurs if the two separate decays are close enough in time to look like a single decay to the electronic system. In this case two detectors measure a coincidence from two separate annihilation events and

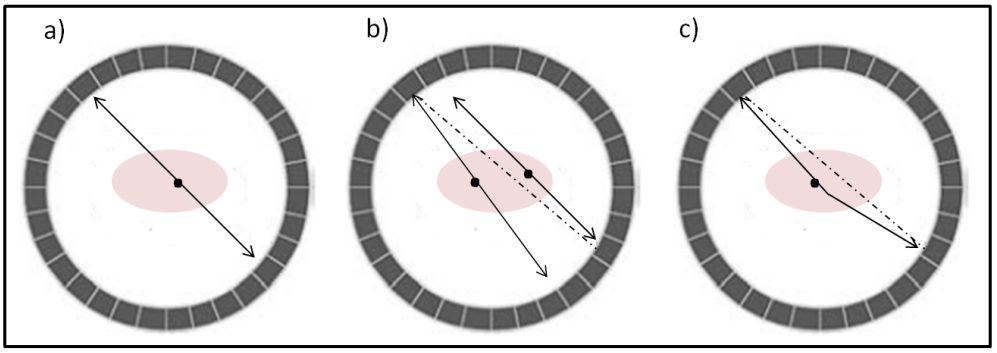

Figure 1.6: Schematic view of coincidences measured by PET detectors

locate this coincidence along a non-existent LOR. It is possible to estimate the number of random coincidences in a given LOR connecting two detectors ($R_{1,2}$) from the coincidence resolving time of the system (τ), the single event rate on the first detector (r_1) and the single event rate on the second detector (r_2) as in equation 1.10:

$$R_{1,2} = 2 \cdot r_1 \cdot r_2 \cdot \tau \tag{1.3}$$

There are two standard approaches to measure and correct accounting for random coincidences:

- Random coincidences estimation: the number of random coincidence for a detector couple is calculated from equation 1.10 and subtracted to the measured coincidences for each detector
- Use of a delayed window: this approach consist in defining another coincidence circuit that has a resolving time grater than τ and that samples random events. These events can be subtracted in real-time or after the use of appropriate variance-reduction techniques

- Scattered Coincidences are sampled when the annihilation photons interact loosing energy in the surrounding tissues and are scattered within the patient. In this case the coincidence will be sampled along a incorrect LOR (see Figure 1.6 c). It is important to correct accounting for scatter events, considering that, in 3D systems, where this problem has a grater impact given the septa absence, the scatter fraction can be as higher as 40% of total sampled events. Using an energy window, part of scattered events can be ignored during the acquisition process. Other scatter correction techniques include integral transform function fitting, energy-based subtraction and analytic calculation [8, 9].

- Spurious Coincidences are spatially uncorrelated counts registered as true events, that can degrade overall quality and quantitative accuracy, due in particular to the use of non pure positron emitters, that is radioisotopes that also emit other high-energy prompt γ-rays in cascade with each other or with the positrons [10].

Attenuation

Annihilation emitted photons travel in surrounding tissue before reaching scintillator detector and undergo a progressive attenuation due to interaction with the crossed media. As consequence, the

effect on the acquisition is that radioactive counts from the inner zones of the scanned object are underestimated.

The attenuation correction can be performed using an image of attenuation coefficient along each LOR acquired with a transmission scan using an external source or a CT scan in the case of PET/CT scanner [11].

Dead time

The dead time is defined as the time needed to complete the process of interaction and detection of the two coincidence photons in PET system. As already reported, this process involve the conversion of the two interacting photons within the detector in light photons, the generation of a pulse within the PMT and the amplification of this pulse by an amplifier. Then the energy and the spatial position of the photon have to be determined and finally the count is recorded if the two events are detected by two detectors in the time window. During the time required to complete the above steps, the detection system is unable to process a second event, which will be lost. This loss (called the dead-time loss) is a serious problem at high count rates, eliminating the possibility to record all the true events.

The dead-time loss can be reduced by using detectors with shorter scintillation decay time and faster electronics components in the PET scanners, or dead time correction can be made by empirically measuring observed count rates at increasing concentrations of activity.

Spatial Resolution

Spatial resolution is empirically defined as the minimum distance between two points that can be imaged by a PET scanner. From a practical point of view spatial resolution refers to the ability of the PET system to image objects depicting the variations in the radioactivity distribution.

Spatial resolution can be characterized by measuring the width of the profile obtained with a point source: the resolution is usually expressed as the full width at half maximum (FWHM) of the profile and the blurring in the image of a point source is referred to as the point spread function of the system.

There are many factors that contribute to the spatial resolution of a PET scanner:

- Positron Range: the positron emitted with residual kinetic energy travels in tissue, losing its energy before annihilation with an electron, thus the site of β^+ emission differs from the site of annihilation
- Non-collinearity of the annihilation photons: if the positron annihilates before losing all its energy, the two 511keV photons are not emitted at exactly 180°, due to residual momentum of the positron at the end of positron range (maximum deviation of $\pm$ 0.25° from 180° direction). As a consequence, the detected LOR does not intersect the annihilation point.
- Detector Resolution (referred as Intrinsic Resolution): the detection system influences the PET resolution (detectors size, distance between detectors, width of the detectors, stopping power of the crystal, incident angle of the photon on the detector, the depth of interaction of the photon in the detector)
- Image Resolution: the process of image generation contributes to the spatial resolution (matrix size, sampling, reconstruction filter, reconstruction method)

Spatial resolution in PET is usually specified in transaxial and axial directions. Transaxial PET resolution for the commercial PET systems generally ranges from 4 to 7 mm and it is often subdivided into radial ($FWHM_r$) and tangential ($FWHM_t$).

Limited spatial resolution of PET system affects quantification of radiotracer uptake in PET images producing the well-kwon Partial Volume Effect that will be extensively covered in the next section.

1.3 Partial Volume Effect

In the previous section it was discussed about the factors that influence the acquired data: all factors are important considering that PET imaging has the potential to produce not only qualitatively accurate images of radiotracer distribution but also quantitatively *in vivo* accurate measurements of tracer concentrations. It was pointed out how the biases introduced by attenuation, random and scatter coincidences, and dead time phenomenon are can now be accounted for, using experimental or analytical method.

On the contrary large biases caused by a physical phenomenon named Partial Volume Effect (PVE) are not accounted for: PVE is not routinely dealt with and is often overlooked, even in clinical research. However accounting for PVE and finding possible way to correct images or quantitative values is essential to quantify PET images in order to evaluate grade of malignancy, to monitor changes in tumor metabolism observing the physiologic response of a tumor to therapy and to correlate PET glucose uptake to proteomic or genomic features of oncological pathologies.

Partial Volume Effect is a phenomenon that causes variations in intensity values of a PET image, making them different from what they really should be. PVE is linked to two different effects.

The first effect, causing PVE, is the image blurring due to the finite spatial resolution of the imaging system. As already explained, the effect of the finite spatial resolution on the image of a point source is not a point on the image but a larger circular source. By a mathematical point of view this effect is described as a 3D convolution operation: the PET image is the result of the convolution between of the actual radiation source with the 3D point spread function of the PET imaging system (see Figure 1.7). The consequence of the 3D blurring causes *spill over* between regions: part of the signal from the source *spills out* in the background (*spill out* effect) and hence is seen outside the actual source, as well as, part of the background surrounding the source spreads into the source (*spill in* effect) (see Figure 1.7).

The second phenomenon affecting PVE is discrete image sampling. Radiotracer distribution is sampled on a discrete voxel grid in which the contours of the voxels do not match the actual contours of the tracer distribution. In this way some voxels include different types of tissues and the signal in each voxel is the mean of the signal of all the included.

1.3.1 PVE consequences on qualitative and quantitative analysis of PET images

PVE can severely affect images both qualitatively and quantitatively.

Consider an hot lesion on a cold background, in two dimension, for the sake of simplicity, as represented in Figure 1.7

As we can see, due to PVE, the imaged lesion maximum value will be lower than the actual maximum value and the lesion volume will appear larger: lesion appears larger but less aggressive than it actually is.

It is hard to recover the activity lost within the actual lesion volume due to the *spill in* effect, as well as that due to the *spill out* effect: in general *spill in* and *spill out* did not compensate each other, therefore, it is difficult to predict the overall effect of PVE.

As a summary

- PVE affects the apparent lesion volume: this effect can be important especially when PET assists in radiotherapy treatment planning

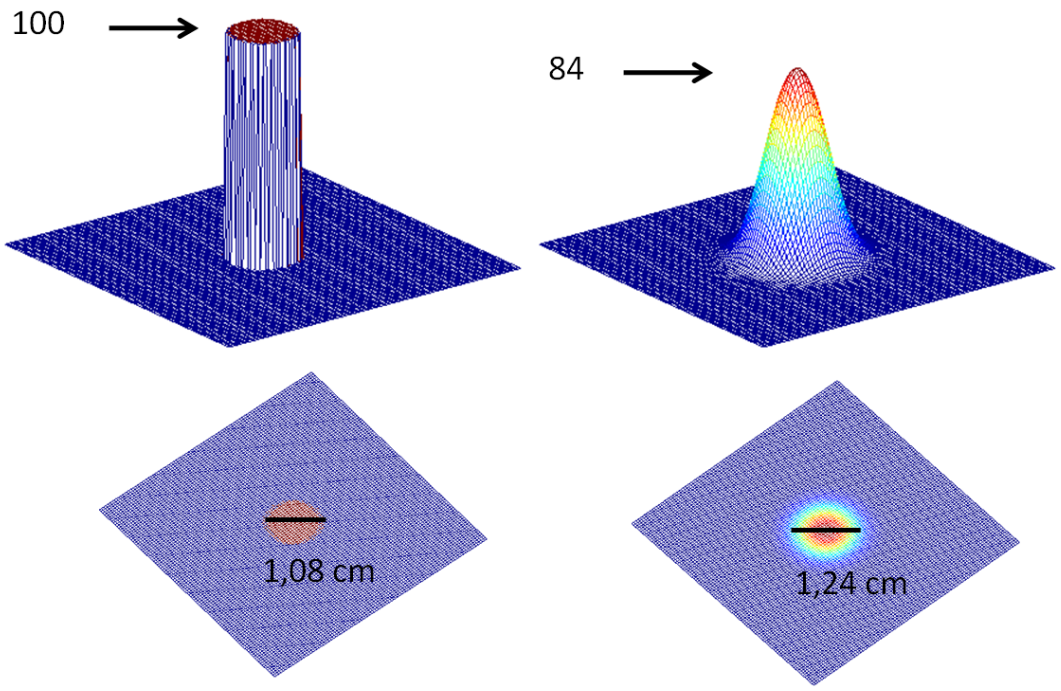

Figure 1.7: Effect of PVE on lesion volume and lesion uptake considering a circular source in two dimensions of uniform activity (100 arbitrary units for lesion uptake, 1,08 cm for lesion volume) in non-radioactive background.

- PVE affects quantification of lesion radioactivity concentration

Underestimation of lesion volume and uptake caused by PVE is more important when lesion are small, typically less than 3 times the full width at half maximum (FWHM) of the imaging system [4]

1.3.2 Parameters affecting PVE

PVE strongly depends on the size of the tumor: lesions with the same uptake but with different volume will be underestimated in a different way, in particular smaller lesions result more affected by PVE than larger lesions. This dependence is extremely confounding when PET images are used to evaluate therapeutic follow-up, bringing to misleading conclusion about the effect of the therapy.

PVE also depends on the shape of the tumor: lesion, with a larger part of the edges exposed to background and thus prone to spilling in and spilling out, are more affected by PVE, that is spherical lesions are less affected then irregular tumors.

The *spill in* phenomenon is dependent on the background activity, so PVE depends on the background activity of the surrounding tissues.

Since the spatial resolution in the reconstructed images determines the signal spreading, it is clear that different PET systems with different spatial resolution will generate a different underestimation effect on the same lesions.

PVE is caused also by the discrete sampling of the counts. It is clear that an image sampling with larger pixels increases the probability of mixing lesion and background tissues underestimating the actual metabolic activity and the actual volume of the tumor.

1.3.3 Effect of Measurement Method on PVE

There is a great interdependency between PVE and the method used to measure lesion volume and lesion uptake.

The topic of measuring parameters such as volume and uptake on PET images is complicated and, at present, there is no consensus regarding how to define the region of interest (ROI) on PET images.

There are different ways used in literature to define ROI on PET images each one with their drawbacks and their merits.

Maximum value ROI

Lesion uptake in ROI can be defined as the maximum value of radioactivity concentration within the lesion. The maximum value is less affected by PVE, but, unfortunately, it is strongly affected by noise. As a consequence, such a measurement technique, in any real imaging situation where noise is always present, makes the uptake highly variable, usually providing an overestimate or an underestimate of the actual maximum pixel value. When used to evaluate metabolic changes during a therapy, the maximum value can lead to misleading conclusions considering that uptake changes may be statistical fluctuations rather than true metabolic changes.

The use of this method do not allow to define, at the same time, a lesion volume, since the defined ROI is a one pixel ROI that do not approximate lesion volume.

The merit of this lesion uptake measurement method is that it is completely independent of the observer and this is why, despite its sensitivity to noise, it is very popular [12, 13, 14].

Manally drawn ROI

Manually drawn ROI can be defined on PET images and, in this case, lesion uptake is calculated as the mean value of uptake in this region, while drawn ROI allows to define a volume. The major drawback of this approach is that both measured uptake value and the defined volume are prone to observer variability.

Fixed-Size ROI

Another way to define lesion uptake is to consider the mean value in fixed-size region, that is to use a ROI of fixed size, regardless of the tumor size, placed centering the ROI around the center of the tumor. This method is operator independent but many biases can be introduced due to the influence of the tumor size. Furthermore, the defined volume clearly can not be considered as an approximation of the actual lesion volume.

ROI Based on Intensity Threshold

A thersholded ROI is an operator independent ROI defined, around the lesion, by an isocontour at a fixed percentage of the maximum pixel value in the tumor: lesion uptake is measured as the mean value within the isocontours. The percentage value are typically between 50% and 80%: the use of too low percentage can bring to include a significant proportion of the background on the defined ROI [15], while the use of high-percentage isocontour increases the noise dependency.

This approach is dependent on the image noise since the defined isocontour depend on the maximum value, that is strongly affected by noise, else if ROI noise dependency on measured lesion uptake is less important since the average operation smooths over signal fluctuations.

Methods that base the isocontour value on the difference between the tumor activity and the background activity can be important to reduce noise dependency [16].

The volume defined by a thresholded ROI do not necessarily match with the actual volume but can be important to define the metabolically active volume of the tumor: the tumor size determined with these approaches is, in fact, a metabolic size, which may disagree with the CT- or MRI-based morphologic size [4, 17].

1.3.4 PVE correction methods

Several techniques have been proposed to compensate for PVE in PET, and exhaustive reviews have compared the different approaches to PVE correction [4, 18].

A general classification of PVE correction methods can be proposed on the basis of their different purposes:

- correction methods performed to obtain PVE-corrected images that allow a quantitative analysis of whole images: these methods give PVE-corrected images that improve the qualitative analysis and that can be used to obtain quantitative PET data
- correction methods performed to achieve PVE-corrected regional values: these methods are applied at a regional level modifying a value measured in a region of the image, to obtain a PVE-corrected value. Such methods do not yield only PVE-corrected images and then are suitable for the quantification of tumor uptake in ROIs, but not for visual analysis.

In the first class we find methods that rely on the joint use of anatomical (CT or Magnetic Resonance Imaging) and functional images and that are applied to reconstructed PET images [19, 20, 21, 3] or applied during reconstruction including the scanner PSF in the reconstruction process [22, 23]. Indeed, this first class of PVE correction, mainly proposed and validated for brain studies [4], can now be considered feasible for whole body studies [24].

In the second class we find the Geometric Transfer Matrix (GTM) method [24, 4], methods based on local deconvolution [4] and the very popular methods based on numerical coefficients (Recovery Coefficient, RC)[4]. In the next section, particular attention will be devoted to extend the discussion about the PVE correction on RC coefficient.

1.3.5 RC-based PVE correction method

RC-based PVE correction methods are based on numerical coefficients (Recovery Coefficient, RC) that are experimental measured using radioactive phantoms and that are used to recover the radioactivity concentration.

Hoffmann in [25] used this approach carrying out PET experimental measurements using radioactive phantoms composed by hot spheres in a cold background. RC coefficients are obtained as the ratio between the PET measured radioactivity concentration and the actual radioactivity concentration within the hot spheres, and RC curves are derived for the actual sphere-to- background ratio as a function of the actual sphere volume. As hot spheres properly simulate metabolic active oncological lesions, the approach was used for PVE correction in PET oncological studies [26]. However, this PVE correction compensated only for the *spill out* of lesion uptake into the background, and did not take into account the *spill in* of the background into the lesion, as actually occurs in body tissues surrounding oncological lesions.

More realistic models combine RC derived from hot spots in a cold background with RC from cold spots in a hot background and hot spots in a warm one, allowing both *spill out* and *spill in* effects to be accounted for example [25].
Even with this extended approach, the applicability of RC-based PVE correction methods to real PET oncological studies is, however, limited by the impossibility of estimating the actual lesion-to-background ratio (L/B) and the actual lesion volume on PET images: in fact, PET images are affected by PVE, and, in *in vivo* patient studies, no a priori information is available for the above parameters [17, 27, 28, 29]. Srinivas SM et al.[30] recently proposed an RC-based PVE correction method for oncological studies using an Operator-Independent (OI) technique to measure lesion radioactivity concentration (C_m), without the need to know the actual L/B. They performed PET measurements of hot spheres in hot background using PET/CT scanner, and obtained RC as a function of measured $(L/B)_m$, derived from an OI technique using maximum pixel value (C_m). However, the major drawback of this approach is that the obtained RC curves were a function of the actual lesion volume of the hot spheres, thus the method was still limited by the need to know the actual lesion volume, one of the major issue in both nuclear medicine and radiology communities. Srinivas SM et al. [30] suggest to use CT-derived volume as an approximation of lesion volume. This is a quite good approximation when lesion density differs from that of the surrounding tissues, but, unfortunately, lesions are not always visible on clinical CT images, and, even if visible, consideration must still be given to any difference between the CT anatomical volume and the PET metabolic volume [31, 32, 33, 15].

1.4 PET image analysis

Clinical application of PET, especially increased after the introduction of PET/CT scanners, which allowed for the collection of both anatomic information and metabolic information *in vivo* in one scanning session [34], is often limited on the possibility to obtain images of the oncological pathologies, visualizing their location and characterizing their features and changes during therapy by a qualitative analysis. In fact, in clinical practice, visual inspection of PET or PET/CT images, based on differences in contrast, is the main tool for image interpretation, and for staging or restaging of oncological pathologies [35]. Despite this, ^{18}F-FDG-PET is inherently a quantitative tool starting from the fact that the FDG uptake is proportional to the glucose consumption, that is to the molecular features that would be imaged by PET. PET quantitative characteristics are increasingly being recognized as providing an objective and more accurate measure than visual inspection alone. In fact, clinicians would take advantage from the possibility of quantifying the ^{18}F-FDG uptake in an oncological lesion in order to characterize the tumor malignancy more accurately and to better monitor any uptake changes after chemotherapy or radiotherapy treatment[36, 37, 38, 39]. Furthermore, in the perspective of personalized medicine and predictive medicine, the availability of *in vivo* quantitative biomarkers for cancer is crucial, and this poses the challenge of integrating *in vivo* and *ex vivo* patient data (e.g PET, histopathologic, protein and gene expression data) [1, 2, 3] to provide individualized prognosis, diagnosis, and therapy.

Considering quantitative analysis of ^{18}F-FDG PET studies, it is possible to distinguish between semi-quantitative parameters and quantitative parameters [40].

Quantitative parameter are those obtained from the analysis of dynamic acquisitions: kinetic PET studies provide a measure of the glucose metabolic rate using the progressive radioactive uptake in tissue and in blood over the time. Dynamic studies require a more complex and time consuming study procedure, with a longer acquisition than static studies and a more complex storage of data (blood sampling, input curve extraction,...).

The difficulties associated with quantitative data on the rate of metabolism of glucose have been overcome using simplified quantitative parameters (semi-quantitative parameters) that are de-

veloped in particular for static acquisition. Semi-quantitative parameters are the Tumor-to-normal tissue ratio (T/N) and the Standardized Uptake Value (SUV) [40].

SUV is the most widely semi-quantitative method for the quantification of PET studies [41] and represents the measured radioactivity concentration of a tissue normalized to a factor, that account for injected activity and body patient characteristics. The resultant number is a crude measure of degree of uptake of FDG into the tissue. Extensive discussion were done about the normalization factor and, at present, three definitions of SUV depending on the normalization factor can be used [6].

Body-weight SUV (SUV_{BW}) is the most widely used definition for the SUV. The normalization is performed dividing the tissue measured activity for the ratio between the injected activity and the body weight, as represented in 1.4:

$$SUV_{BW} = \frac{TissueRadioactivityConcentration(MBq/cc)}{\frac{InjectedActivity(MBq)}{BodyWeight(g)}} \tag{1.4}$$

Body Surface Area (BSA) normalization factor account for both the weight and the height of the patient as represented the 1.5 and 1.6 formula:

$$SUV_{BSA} = \frac{TissueRadioactivityConcentration(MBq/cc)}{\frac{InjectedActivity(MBq)}{BSA(m^2)}} \tag{1.5}$$

$$BSA(m^2) = 0.007184 \cdot weight^{0.425} \cdot height^{0.725} \tag{1.6}$$

Lean Body Mass (LBM) SUV uses as normalization factor the ratio between the injected activity and the lean body mass index, whose definition is different for male and female patients, as represented in 1.7, 1.8 and 1.9 formulas:

$$SUV_{LBM} = \frac{TissueRadioactivityConcentration(MBq/cc)}{\frac{InjectedActivity(MBq)}{LBM(kg)}} \tag{1.7}$$

$$MaleLBM(kg) = 48 + 1.06 \cdot [height - 152] \tag{1.8}$$

$$FemaleLBM(kg) = 45.5 + 0.91 \cdot [height - 152] \tag{1.9}$$

As a quantitative parameter, SUV is affected by PVE, but it is also dependent from blood glucose level and from interval between the injection and the start of acquisition: in order to obtain reliable SUV values it is very important to account for all these parameters

1.5 PET radiotracers and radiopharmaceuticals

There are several positron-emitting radioisotopes that are used for PET imaging.

Two principal methods are used for the production of radioisotopes: they can be produced from bombardment of a target material by charged particles in an accelerator or they can be obtained starting from the decay of a generator nucleus.

Radioisotopes are prepared to label molecular compounds to produce the radiotracers that are injected into the body and that make biological processes visible to PET scanner.

Table 1.2 show a short list of some positron-emitters with their physical characteristics and the associated radiopharmaceutical with its clinical application.

As we can see, some radioisotope are very important elements for biological systems (carbon, nitrogen, oxygen), this makes easy to label molecules involved in biological process with the radioactive isotope.

Table 1.2: Physical characteristics of some PET radiotracers with the clinical used radiopharmacetutical

Nuclide	Physical half-life (min)	Common production method	Radiopharmaceutical	Clinical applications
$^{11}_{6}$C	20.4	Cyclotron	^{11}C-Carbon monoxide	Plasma volume
			^{11}C-choline	Phospholipids biosynthesis
$^{13}_{7}$N	10	Cyclotron	^{13}N-ammonia	Blood flow
$^{18}_{9}$F	109.8	Cyclotron	^{18}F-FDG	Glucose metabolism
			^{18}F-FLT	DNA proliferation
			^{18}FMISO	Hypoxia
$^{15}_{8}$O	2	Cyclotron	^{15}O-water	Blood flow
$^{82}_{37}$F	72 s	Precursor	^{82}Rb-chloride	Myocardial perfusion

Characteristics of an ideal radiotracer are listed below:

- The radiotracer has not alter the studied biological process, that is the radiopharmaceutical has to have the same behavior in tissues of the natural compound
- The radiotracer half-life has to be longer enough for accounting the production time and shorter enough to ensure a reasonable acquisition time for clinical studies
- The radiotracer quantity has to be similar to that of natural compound
- The radiotracer activity has to give a sufficient signal

The most used and developed radiopharmaceutical for oncological studies is ^{18}F-fluorodeoxyglucose.

^{18}F-fluorodeoxyglucose

One of the more used radioisotope for oncological purposes is the fluorine-18. The fluorine-18 is typically produced by a nuclear reaction with oxygen

$$^{18}O(p,n)^{18}F \tag{1.10}$$

At high-energy proton interacts with the ^{18}O nucleus and, as consequence, a neutron is emitted, leaving a fluorine-18 isotope.

The development of radiotracers using ^{18}F was promoted by the evidence that many cancers are associated with a high glucose metabolic rate [42, 43]. ^{18}F-FDG is an analogue-to-glucose molecule, obtained with replacement of the oxygen in C-2 position with 18-fluorine. Following intravenous injection ^{18}F-FDG is transported across the cell membrane by sodium independent, facilitative glucose transporters (Gluts), that allow energy independent transport of glucose across the cell membrane down a concentration gradient [44]. Intracellularly, both ^{18}F-FDG and glucose are phosphorylated by hexokinase to glucose-6-phosphate and ^{18}F-FDG-6 phosphate, respectively. While glucose-6 phosphate is further metabolized to fructose-1,6-biphosphate and enters glycolysis, ^{18}F-FDG- 6-phosphate cannot be further metabolized in the glycolytic pathway because the F atom at the C2 position prevents ^{18}F-FDG-6P from further degradation. As the cell membrane is impermeable for phosphorylated ^{18}F-FDG, ^{18}F-FDG-6 phosphate becomes trapped and steadily

accumulates in metabolically active tumor cells. Although ^{18}F-FDG undergoes only two glycolysis step ^{18}F-FDG uptake rates reflect exogenous glucose utilization of cancer cells, as long as patients are imaged at steady-state conditions. ^{18}F-FDG is not reabsorbed after glomerular filtration, but excreted with the urine because ^{18}F-FDG is not a substrate for the sodium dependent glucose transporters found in the tubulus system of the kidneys. This contributes to the rapid clearance of this radiotracer from the blood stream which is a very important characteristic for imaging metabolically active tissues with high contrast.

1.6 *In vivo* and *ex vivo* data integration

Considering oncological pathologies, both *in vivo* and *ex vivo* molecular imaging are important to understand cancer features and to orient the therapy in the correct direction for each patient.

Between the *ex vivo* techniques, proteomics, genomics, metabolomics and the more classical histopathology have an important role in the research of molecular features and molecular alterations at the origin of cancer pathologies. In recent years, tremendous advances have been made in *in vitro* tissue analysis techniques. With the successful mapping of the human genome and the rapidly advancing high-throughput technologies, the quantification of the level of expression of genes and many different proteins from tissue samples have been obtained. Despite recent progress and advance, clinical translation of those technologies is still faraway, due to their high cost and to long time required for the analysis.

At the same time, ^{18}F-FDG PET is a very useful molecular imaging tool to study oncological pathologies *in vivo*, in a non-invasive way, taking advantage from the increased glucose uptake of tumor cells. This technology is already changing the management of many diseases, including cancer, where it can define different aspects of disease (morphology, function, biochemistry) in a high accurate manner.

Notwithstanding both these *ex-vivo* and *in-vivo* molecular imaging techniques are showing increasing potential in identifying biomarkers for the detection of cancer disease, in addressing patients to the therapy treatment and in monitoring disease and therapy effects, these two methodologies have not fully explored and need to be integrated in order to understand the complexity of biologic processes behind oncological pathologies.

Proper techniques to perform the integration between these approach to oncological pathologies are not yet available. Encouraging results have come from two recently published studies of oncological patients [1, 2, 3], devoted to the integration of genomic data with PET and CT data, respectively. Both studies show that qualitative or quantitative or semi-quantitative parameters obtained from lesions on *in vivo* images (anatomical or functional) systematically correlate with much information relative to gene expression profiles. These results, obtained by the use and optimization of sophisticated data analysis including bioinformatics and biostatistics, make concrete the possibility of an integration for *ex vivo* and *in vivo* molecular imaging and open the possibility to bring to a more accurate diagnostic approach, simplifying the comprehension of the multi-factorial origin of some diseases.

Chapter 2

Quantification techniques for PET/CT whole-body oncological studies with RC-based Partial Volume Effect correction

2.1 Aim

Aim of this first part of the PhD work was the development and the implementation of an easy, accurate and clinically feasible method to quantify radiotracer uptake for PET/CT oncological studies, with Partial Volume Effect correction.

2.2 Materials

2.2.1 ^{18}F-FDG and PET/CT studies

^{18}F was produced by a cyclotron (RDS Eclipse, Siemens Healthcare) with a fixed proton beam of 11 MeV. ^{18}F-FDG synthesis was obtained by nucleophilic substitution in acidic medium and subsequent purification. A dose measurement system (Dose calibrator Pet Dose, Comecer) provided measurements of the amount of ^{18}F-FDG radioactivity (administered and residual) for both phantom and patient studies. For the phantom studies, the radioactivity concentration measured by the dose calibrator was assumed as the *Gold Standard* radioactivity concentration (C_{GS}).

PET/CT measurements were performed on the multi-modal PET/CT system "Discovery STE" (General Electric Medical Systems) [45] installed in the Nuclear Medicine Department of the Scientific Institute H San Raffaele. The PET/CT system was cross-calibrated with the dose measurement system.

All the PET/CT studies (on both phantom and patients) were performed according to the oncological clinical protocol of the Discovery STE scanner: the oncological protocol includes a SCOUT scan at 40 mA, a CT scan at 140 keV and 150 mA (10 sec), and 3D PET scans (2.5 min/scan) for adjacent bed positions.

PET images were reconstructed by a 3D ordered subset expectation maximization algorithm (OSEM, 28 subsets, 2 iterations, 5.14 mm Gaussian post-smoothing) with corrections for random, scatter and attenuation incorporated into the iterative process. For each bed position the PET image volume consisted of 128 x 128 x 47 voxels of 4.7 x 4.7 x 3.27 mm^3 size, while the CT volume was 512 x 512 x 47 voxels of 0.97 x 0.97 x 3.27 mm^3 size. The transaxial spatial resolution

of the PET system (FWHM), for the above mentioned OSEM reconstruction with the Gaussian post-smoothing, is 6.36, 6.45, 6.61, 6.93, 7.41 mm at 0, 5, 10, 15 and 20 cm from the centre, respectively.

2.2.2 Phantom studies

Several phantoms were used for different purposes.

The NEMA 2001 IQ phantom, consisting of six spheres of different volumes ($d_1 = 10mm, d_2 = 13mm, d_3 = 17mm, d_4 = 22mm, d_5 = 26mm, d_6$ = 37 mm), positioned at 5,5 cm from the center of the phantom, inside an elliptical cylinder (D1 = 24 cm, D2 = 30 cm, h = 21 cm) [46], was used to estimate the severity of the Partial Volume Effect (PVE) (in terms of underestimation in the radioactivity concentration), for the considered PET system and study protocol, and to determine the RC curves for the considered PET/CT system. The six spheres and the background were filled with ^{18}F-FDG. The actual sphere-to-background ratio (S/B_{GS}) obtained by the dose calibrator ranged from 4 to 35 for 15 independent experiments while the background concentration ranged from 0.002 MBq/ml to 0.02 MBq/ml.

Three anthropomorphic phantoms, simulating different body regions (brain, thorax, breast), filled with spheres (diameter = 9.8, 12.3, 15.6, 25.8, 31.3 mm), simulating oncological lesions, were used to evaluate performance and accuracy of the developed PVE correction method.

The Hoffman 3D Brain phantom [47] was used for the validation of the PVE correction method in the brain district. The three smallest spheres were inserted in the phantom in the cerebellum and in the anterior cortex.

A thorax phantom (elliptical cylinder, d_1 = 20 cm, d_2 = 30 cm, h = 21 cm) with two cork parts simulating lungs and a cardiac insert was used for the validation of the PVE correction method in the thorax district. All the five spheres were inserted in the mediastinum part of the thorax phantom.

A breast phantom was assembled using the previously described thorax phantom (no cardiac insert) and two plastic containers (cylinder equivalent radius = 3 cm, h = 10 cm) miming breasts. All the five spheres were inserted, in different experiments, in the containers.

Figure 2.1 shows the anthropomorphic phantoms.

Figure 2.1: The anthropomorphic phantoms: the Hoffman 3D brain phantom (left), the thorax phantom (center), the breast phantom (right)

The spheres and the background were filled with ^{18}F-FDG, so that $(S/B)_{GS}$ obtained by the dose calibrator ranged from 4 to 35 for 15 independent experiments (the actual radioactivity concentration in the background ranged from 0.002 MBq/ml to 0.008 MBq/ml).

2.2.3 Patient studies

Two different group of patients were used to evaluate the feasibility and the effect of PVE correction on PET/CT oncological studies.

For both groups, a particular care was devoted to measure accurately patient data (weight and height) as well as PET/CT study data (administered and residual dose, time between injection and the start of acquisition, glycemia), in order to obtain a correct value of the Standardized Uptake Value (SUV).

Follow up patients

In the first group patients with several oncological diseases were selected with the purpose to evaluate the clinical feasibility of the PVE correction methods and the effect on the response to treatment.

In particular a total of sixteen oncological patients (6 men, 10 women; mean age 57 years; age range: 40-76 years) was selected. Each patient performed two separate PET/CT studies, a basal study and a follow up study, after a therapy treatment (Chemotherapy, Tomotherapy, Oncological Drugs, Chemotherapy and Tomotherapy, Oncological Drugs & Tomotherapy).

Patients fasted for twelve hours before the exam and were intravenous injected with ^{18}F-FDG (1mCi/10kg). Patients waited approximately one hour after the injection and a PET/CT study was performed, following the whole-body oncological protocol. A total of 24 oncological lesions were considered: among the considered lesions, 9 were primitive carcinomas, 15 were metastasis or lymph node relapses.

The characteristics of the considered patients are presented in Table 2.1.

Breast cancer patients

In the second group patients with breast cancer were considered and recruited within patients enrolled in a specific "integration protocol" explained in the next chapter: the effect of PVE correction on the absolute Body-Weight Standardized Uptake Value (SUV_{BW}) was evaluated.

Specifically, a total of twelve women (mean age: 61 years; age range: 38-80 years) were selected by a breast surgeon. Each patient performed a basal PET/CT studies, before surgery.

2.3 Methods

2.3.1 The measurement techniques for V_m and C_m

We considered both Operator-Dependent (OD) and Operator-Independent (OI) techniques to perform measurement of lesion volume V_m and lesion uptake C_m at the regional level on PET/CT images.

By the OD_{max-CT} technique, V_m is obtained from a manually drawn region of interest (ROI) placed around the lesion, on the CT image. Radioactivity concentration C_m is obtained, once V_m is correctly copied on the co-registrated PET image, as the maximum value of radioactivity concentration within V_m.

By the $OD_{max-PET}$ technique, V_m is obtained from a manually drawn ROI placed around the lesion, on the PET image. C_m is obtained as the maximum value of radioactivity concentration within V_m.

By the $OD_{mean-CT}$ technique, V_m is obtained from a ROI manually drawn around the lesion on the CT images, as for the the OD_{max-CT} technique. C_m is obtained, once V_m is copied on the co-registered PET image, as the mean value of radioactivity concentration within V_m.

By the $OD_{mean-PET}$ technique, V_m is obtained from a ROI manually drawn around the lesion on the PET images and C_m is obtained as the mean of radioactivity concentration within V_m.

Table 2.1: FOLLOW UP PATIENTS CHARACTERISTICS

Patient number	Age (y)	Sex	N° of of	Location	Follow up period (m)	Cancer Diagnosis	Treatment
1	76	F	3	Abdomen	7	Metastasis from ovarian cancer	Chemotherapy
2	53	F	1	Liver	6	Metastasis from ovarian cancer	Chemotherapy and Tomotherapy
3	40	F	2	Pharynx	6	Head and neck cancer	Chemotherapy and Tomotherapy
4	51	F	2	Abdomen	3	Pancreas cancer	Chemotherapy and Tomotherapy
5	59	F	1	Bone	7	Metastasis from mesothelioma	Chemotherapy
6	71	M	1	Liver	10	Metastasis from pancreas carcinoma	Chemotherapy and Tomotherapy
7	61	F	1	Sternum	2	Metastasis from breast cancer	Chemotherapy and Oncological Drugs
8	42	M	2	Bone	3	Metastasis from melanoma	Tomotherapy
9	56	M	1	Abdomen	5	Pancreas cancer	Chemotherapy and Tomotherapy
10	55	F	1	Oesophagus	5	Oesophagus cancer	Tomotherapy
11	59	F	2	Breast	10	Breast cancer	Oncological Drugs
12	47	M	1	Stomach	5	Stomach cancer	Chemotherapy
13	50	F	2	Bone	9	Metastasis from breast cancer	Oncological Drugs
14	46	M	1	Mandible	2	Head and neck cancer	Chemotherapy
15	70	F	1	Liver	6	Cholangiocarcinoma	Chemotherapy
16	68	M	2	Tonsil	6	Head and neck cancer	Chemotherapy and Tomotherapy

By the $OI_{max-PET}$ technique, V_m is obtained from a ROI automatically drawn around the lesion on the PET image using an isocontour at a fixed threshold of the maximum value of radioactivity concentration. C_m is obtained as the maximum value of radioactivity concentration within V_m.

By the $OI_{mean-PET}$ technique, V_m is obtained from a ROI automatically drawn around the lesion on the PET image using an isocontour at a fixed threshold of the maximum value of radioactivity concentration. C_m is obtained as the mean radioactivity concentration within V_m.

Different threshold value (40%, 45%, 50%, 55%, 60%, 65%, and 70%) were explored for both the $OI_{max-PET}$ and $OI_{mean-PET}$.

PET/CT studies of the NEMA IQ 2001 phantom allow to assess the performance of the measurement techniques: experimental measurements were carried ou so that in each experiment all the spheres showed the same $(S/B)_m$. C_m value was calculated for each sphere of the phantom, according to the measurement techniques and $(S/B)_m$ was obtained as the ratio between the PET measured sphere uptake C_m and the PET measured radioactivity background surrounding the spheres, calculated as average over twenty circular ROIs.

C_m value was compared with the actual radioactivity concentration C_{GS}, in terms of percentage difference between C_{GS} and C_m for different $(S/B)_m$.

Table 2.2 summarizes the characteristics of each measurement technique.

Table 2.2: MEASUREMENT TECHNIQUE CHARACTERISTICS

Technique	V_m	C_m
OD_{max-CT}	Manually drawn on CT image and copied on the PET image	Max value within V_m
$OD_{max-PET}$	Manually drawn on PET image	Max value within V_m
$OD_{mean-CT}$	Manually drawn on CT image and copied on the PET image	Mean value within V_m
$OD_{mean-PET}$	Manually drawn on PET image	Mean value within V_m
$OI_{max-PET}$	Automatically drawn on PET image by a threshold isocontour from the maximum	Max value within V_m
$OI_{mean-PET}$	Automatically drawn on PET image by a threshold isocontour from the maximum	Mean value within V_m

Optimization of the OI technique

In order to optimize the threshold for the OI techniques, a comparison between the actual and the PET measured active volume was performed.

PET measured metabolic volumes were calculated on the PET images according to the described OI techniques for thresholds at 40%, 45%, 50%, 55%, 60%, 65%, 70% of the maximum sphere uptake. The percentage differences between the actual sphere diameter and the measured sphere diameter derived using different threshold were calculated.

The optimal threshold was chosen as the threshold giving the lowest positive percentage difference: this warrants the actual sphere metabolic volume to be represented as well as possible by the PET measured volume excluding, at the same time, background components.

2.3.2 RC curves

RC were calculated, for each sphere of the NEMA 2001 IQ phantom, as the ratio between $(S/B)_m$ and $(S/B)_{GS}$.

C_m was measured according to the considered measurement techniques. For each measurement technique and for each sphere, $(S/B)_m$ was obtained by the ratio between the PET measured C_m

and the PET measured radioactivity background surrounding the spheres, measured as average over twenty circular ROIs. The background was assumed not to be affected by PVE.

For each of the measurement technique, RC curves were obtained by fitting RC experimental data for fixed $(S/B)_m$ as a function of the ratio between measured sphere diameter (d_m) and system FWHM, with a three parameters hyperbolic function (see Equation 2.1).

$$f(x) = a \cdot \left(\frac{x}{x+b}\right)^c \quad \text{where x} = \frac{d_m}{FWHM} \tag{2.1}$$

It is important to obtain RC curves normalizing d_m to the PET scanner FWHM, because it is possible to account for the effect of the location of quantified object. In fact all the NEMA IQ phantom spheres are place at the same radial distance (5.5 cm) from the center of transaxial field of view and at the same axial location, then the spatial resolution is the same for all the spheres, while in real clinical PET/CT studies oncological lesion can be placed everywhere in the transaxial field of view.

A set of RC curves as function of d_m at different $(S/B)_m$ can be used to correct for PVE. Once the location of the sphere/lesion is obtained, in terms of radial distance from the center of field of view, the FWHM corresponding to the sphere/lesion location can be determined. Measurement of sphere/lesion $(S/B)_m$ allows to select the correct RC curve and the RC value corresponding to the measured d_m/FWHM value can be used to correct C_m and SUV_m, dividing the affected values for the derived RC value.

RC noise sensitiveness

The sensitiveness to noise level on the PET images was assessed. PET/CT measurements were performed with the NEMA IQ phantom, following oncological protocol but using different acquisition times (2.5 min, 5 min, 10 min, 15 min, 30 min). For each sphere, RC was calculated at each acquisition time and percentage differences of RC over time was obtained.

2.3.3 Accuracy of the PVE correction method

The accuracy of the PVE correction method was assessed from the PET/CT studies of the anthropomorphic phantoms.

For each sphere of the anthropomorphic phantoms, measurements of C_m and d_m were performed with each measurement techniques. The $(S/B)_m$ value was derived measuring the background radioactivity concentration as average over, at the most, 4 circular ROI. Variation Coefficient (CV) was measured in the same background region, in order to estimate the uniformity of radioactivity background. A proper RC was obtained dependently from those $(S/B)_m$ and d_m derived by each of the measurement techniques, accounting for the sphere location.

The residual error, before and after applying PVE correction, estimated as percentage difference between C_{GS} and corrected C_m (corrected C_m = C_m/RC), was derived for each of the six measurement techniques, with all the anthropomorphic phantoms.

2.3.4 Quantification tool

At present there are many both commercial and open sources software packages to analyze PET/CT images, such as Xeleris GE, and ImageJ [48]. These tool satisfy qualitative analysis, but they did not allow quantitative analysis with PVE correction, they did not support collaborative process [49, 50], and they did not allow code manipulation.

In order to perform PET/CT quantification with the PVE correction, a proper software, called Couch (Correlative and Collaborative Touch System) , that overcomes these limitations, was developed to visualize and analyze PET/CT images; cOuch was designed for PET/CT qualitative and quantitative reporting, it includes tools for interactive image visualization, optimal manual and semiautomatic region definition, standardized uptake value measurements with partial volume correction. This software encourages easy diagnostic reporting with free-hand text and annotations for telemedicine, and it is based on a low cost touchscreen technology. Furthermore, many functionality are devoted to the research of correlation between PET/CT quantitative parameters and clinical, hystological and proteomic data.

cOuch was developed in MATLAB R2008a that has simplified maintenance, maximized adaptability and reduced time for new procedures development. An accurate description of cOuch is presented in Appendix A.

2.3.5 Clinical application of the PVE correction method

The clinical feasibility of the PVE correction methods was assessed from the oncological patient PET/CT studies. In fact the measured RC curves, used to correct for PVE, are obtained under defined assumption: in particular RC values were obtained for spherical object, with an uniform uptake for a defined range of sphere d_m and $(S/B)_m$.

Criterium to evaluate clinical feasibility was to consider, for each considered lesion, and for each patient, the following four parameters:

- Number of lesions whose measurement of V_m and C_m was reliable for each of the measurement technique (reliability of each measurement technique);
- Number of lesions with V_m and $(L/B)_m$ within the range of sphere V_m and $(S/B)_m$ of the RC curves (reliability of the measured RC curves);
- Number of lesions with uniform uptake: the uniformity was evaluated as satisfied if one single peek, within the lesion, was visually detected on the histogram of image voxel values by all the operators (uniformity requirement);
- Number of lesions with spherical shape: the roundness was evaluated as satisfied when the percentage difference between the maximum and the minimum lesion diameter with respect to the maximum lesion diameter, measured on the PET transaxial, coronal and sagittal images, was found < 50% from all the operators (roundness requirement).

Quantitative analysis was performed by calculating, for each considered lesion, the Body-Weighted SUV, before (SUV_{BW}) and after PVE correction (PVE-corrected SUV_{BW}), for both basal and follow up studies for follow up patients and for basal study for breast cancer patients. The background was measured as average over a maximum of four circular ROIs. Variation Coefficient (CV) was measured in the same background region, in order to estimate the uniformity of radioactivity background.

The effect of the location of the lesion of the patients was taken into account by normalizing each d_m to the PET image spatial resolution, expressed as FWHM at the lesion location.

For follow up patients, SUV_{BW} variations during follow up (δSUV_{BW}) were calculated, before and after PVE correction. A paired t-test was performed to compare SUV_{BW} distributions before and after PVE correction, both in basal and follow up studies, as well as δSUV_{BW} distributions before and after PVE correction.

For breast cancer patients, SUV_{BW} before surgery was calculated, before and after PVE correction. A paired t-test was performed to compare SUV_{BW} distributions before and after PVE correction.

2.4 Results

2.4.1 Measurement techniques

PET/CT independent measurements with the NEMA IQ phantom were performed according to the oncological protocol, using an acquisition time of 30 min/scan in order to minimize the noise level on the PET images, in order to evaluate the severity of PVE with respect to the different measurements techniques.

The radioactivity underestimation

The expected severity of the error caused by PVE was confirmed from the results of the NEMA IQ phantom.

As general result, smaller is the object, grater results the radioactivity underestimation. In particular considering both the OD and OI measurement techniques, the radioactivity underestimation ranges from a minimum of 20% for larger sphere to a maximum of 78% for the smaller sphere.

Table 2.3 shows the percentage difference between expected (C_{GS}) and measured radioactivity concentration (C_m) for all the spheres of the NEMA IQ phantom and for the minimum S/B_{GS} (S/B_{GS} = 4-6), considering the OD measurement techniques.

In particular for the $OD_{mean-CT}$ and the $OD_{mean-PET}$ techniques, C_m was evaluated by ROIs drawn by three different operator, then the errors in Table 2.3 were obtained as standard deviation of values measured by the different operators.

Table 2.3: RADIOACTIVITY UNDERESTIMATION FOR THE OPERATOR DEPENDENT (OD) MEASUREMENT TECHNIQUES

d_{GS} (cm)	$\% \frac{(C_m - C_{GS})}{C_{GS}}$			
	OD_{max-CT}	$OD_{max-PET}$	$OD_{mean-CT}$	$OD_{mean-PET}$
1	62.5	62.5	77.7 ± 7.9	78.3 ± 0.7
1.3	38.0	38.0	57.0 ± 2.0	66.9 ± 1.6
1.7	24.1	24.1	$46.6 \pm 4{,}1$	57.3 ± 0.7
2.3	22.4	22.4	44.4 ± 5.4	51.7 ± 2.3
2.9	23.4	23.4	42.9 ± 0.1	47.4 ± 2.1
3.7	19.6	19.6	38.4 ± 1.6	42.4 ± 2.1

As expected, for the OD_{max-CT} and the $OD_{max-PET}$ techniques the underestimation values are presented without errors since all the operators measured the same maximum value of C_m. Furthermore, both the ROIs drawn on PET image and on CT image give the same C_m value confirming that the maximum value is always correctly measured.

Table 2.3 shows that the underestimation obtained by OD techniques using the maximum value is less important than that of the OD techniques using the mean value. In fact, as already pointed out in the previous chapter, the maximum uptake value is less affected by PVE even if it can be strongly affected by image noise.

Table 2.3 shows also that the underestimation decreases with the increase of the sphere dimensions; this trend is not observed for the OD_{max-CT} and the $OD_{max-PET}$ in the sphere n°5, probably due to the noise dependency of the maximum uptake value.

Comparing the underestimation values obtained by the $OD_{mean-CT}$ and the $OD_{mean-PET}$ techniques, the $OD_{mean-CT}$ technique shows a better performance with respect to the $OD_{mean-PET}$

technique, except for the smallest sphere, where the better image resolution of CT-based V_m with respect to PET-based V_m is ineffective.

The radioactivity underestimation for the OI_{max} technique and for the explored threshold was found to be the same of the OD_{max-CT} and $OD_{max-PET}$, as expected considering that all these techniques use the maximum uptake value as measure of C_m.

Table 2.3 show the percentage difference between C_{GS} and C_m for all the spheres of the NEMA IQ phantom and for the minimum S/B_{GS} (S/B_{GS} = 4-6), considering the $OI_{mean-PET}$ technique with threshold ranging from 40% to 70%.

Table 2.4: RADIOACTIVITY UNDERESTIMATION FOR THE $OI_{mean-PET}$ MEASUREMENT TECHNIQUE

d_{GS} (cm)	$\% \frac{(C_m - C_{GS})}{C_{GS}}$						
	$OI_{mean-40\%}$	$OI_{mean-45\%}$	$OI_{mean-50\%}$	$OI_{mean-55\%}$	$OI_{mean-60\%}$	$OI_{mean-65\%}$	$OI_{mean-70\%}$
1	59.4	77.5	72.9	71.6	70.3	67.2	63.7
1.3	60.7	56.6	54.5	51.0	48.6	44.3	36.6
1.7	49.6	45.9	43.3	42.2	39.0	35.3	33.4
2.3	47.2	42.8	40.9	40.5	37.4	34.6	31.6
2.9	47.0	44.0	41.4	40.0	39.6	38.1	35.2
3.7	39.1	36.3	34.3	32.6	31.9	30.6	29.1

Observing the trend obtained with the $OI_{mean-PET}$ technique, the radioactivity underestimation decrease with the increase of the threshold value, considering that grater is the threshold, closer is the mean value to the maximum uptake value.

Underestimation results confirm that PVE correction is mandatory for accurate quantification of PET data.

Optimization of the OI technique

Both the OI techniques using maximum or averaged uptake value define the same metabolic volume.

In graphs in figure 2.2, the percentage difference between d_{GS} and d_m is represented as a function of the used threshold, for three different intervals of $(S/B)_m$

The threshold that allows to obtain the better approximation of the actual volume, without overestimate it for all the spheres and for each considered $(S/B)_m$ is the 60% threshold. The threshold at 60% of the maximum value was used as the optimal threshold.

2.4.2 RC curves

Figures 2.3, 2.4, and 2.5 show RC curves obtained for each considered measurement technique.

Experimental RC values were fitted with a three-parameter hyperbolic function and the fit was accurate for all the obtained set of curves (R-square > 0.97).

For all the obtained sets, we found that for a fixed value of lesion diameter the RC values increase with the increase of the $(S/B)_m$ value.

As expected for many sets, the obtained fit is not accurate for less than 1.2, due to the absence of experimental values: in this case PVE correction remains not so accurate trustworthy.

Using the maximum value as a measure of C_m, the RC curves were obtained only for $(S/B)_m$ less than 20. In fact for $(S/B)_m$ grater than 20, RC values were founded grater than 1: in this case,

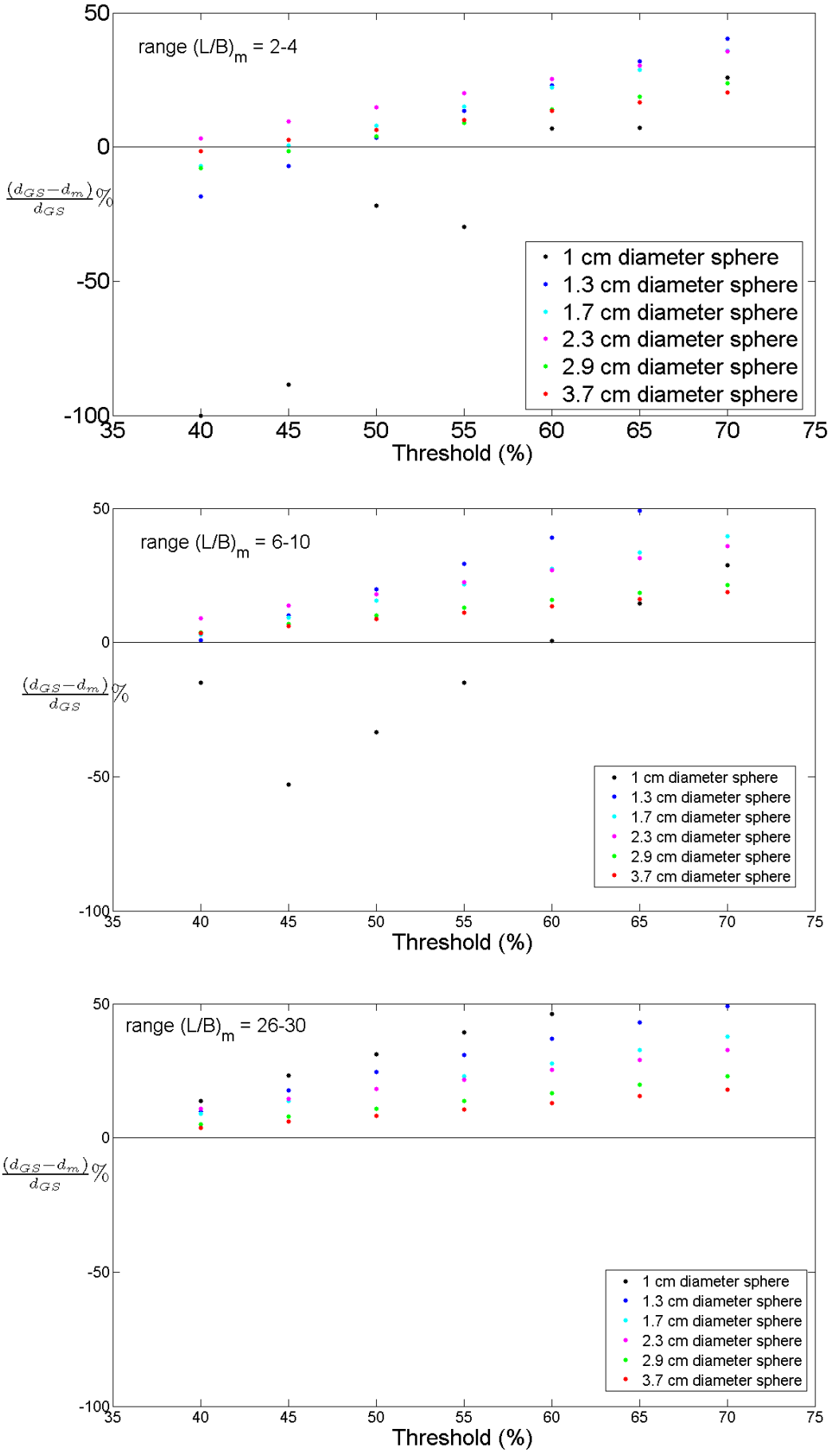

Figure 2.2: Percentage difference between d_{GS} and d_m for different $(S/B)_m$ values

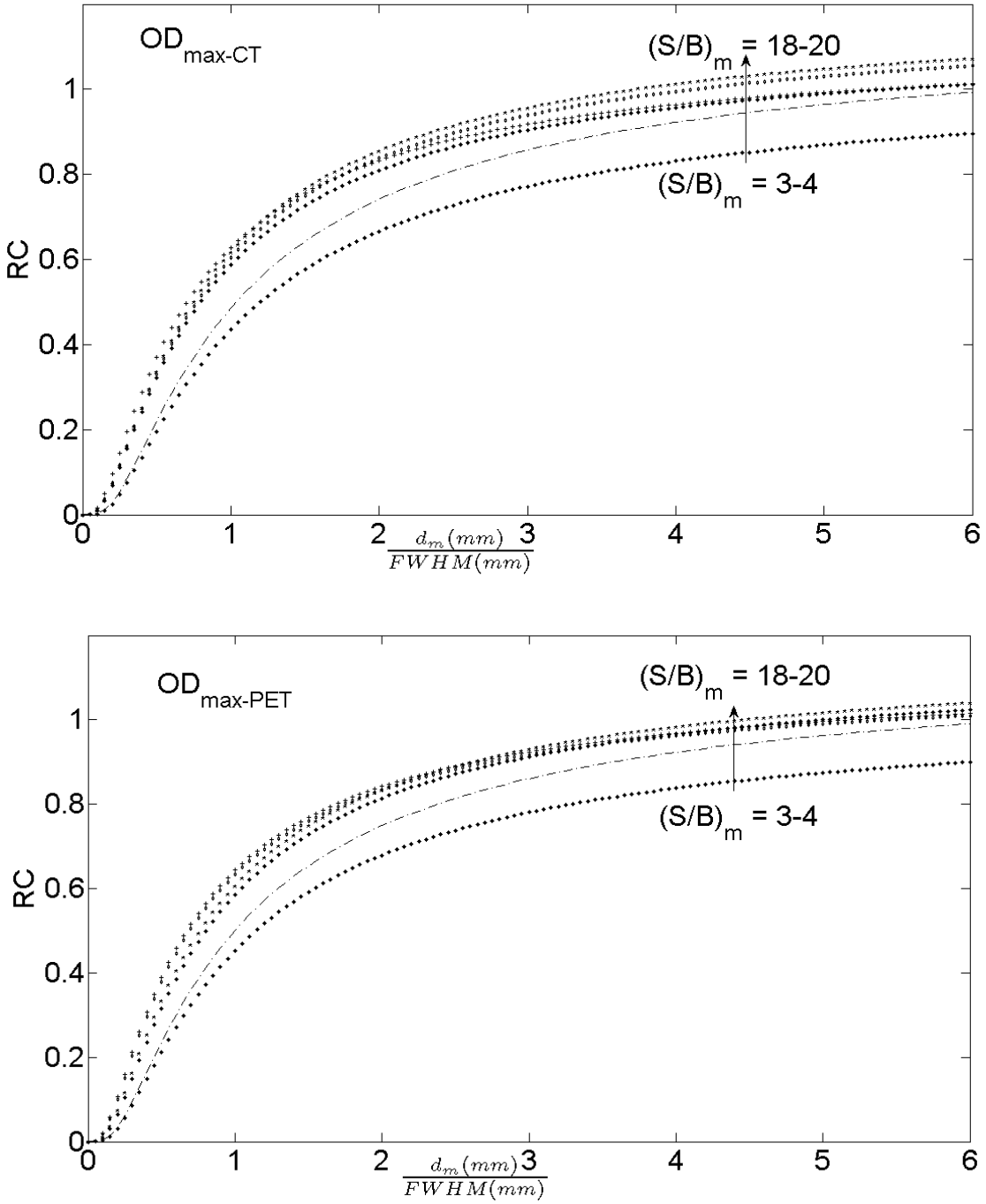

Figure 2.3: Set of RC curves for the OD $_{max-CT}$ and OD $_{max-PET}$ measurement techniques

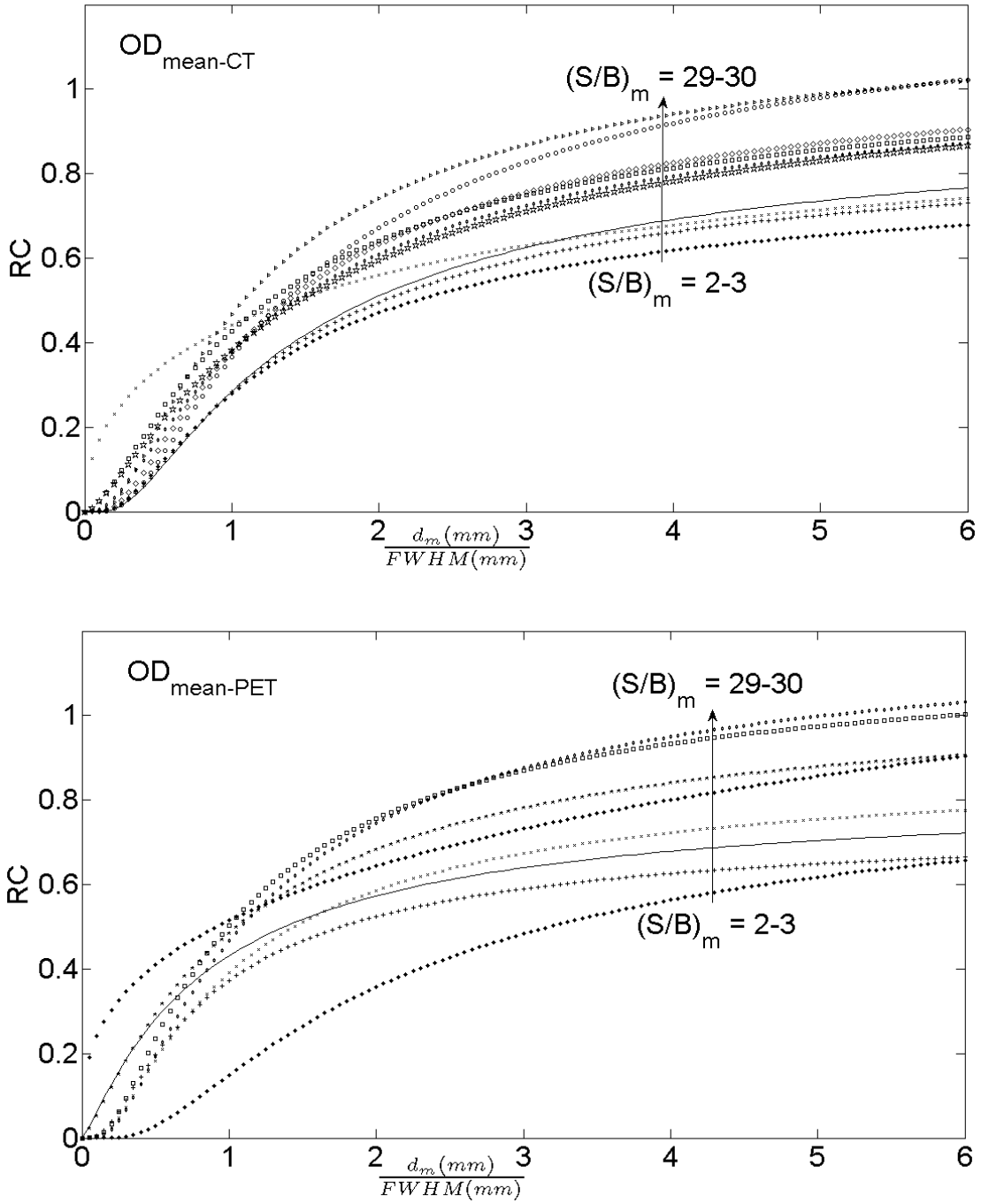

Figure 2.4: Set of RC curves for the OD $_{mean-CT}$ and OD $_{mean-PET}$ measurement techniques

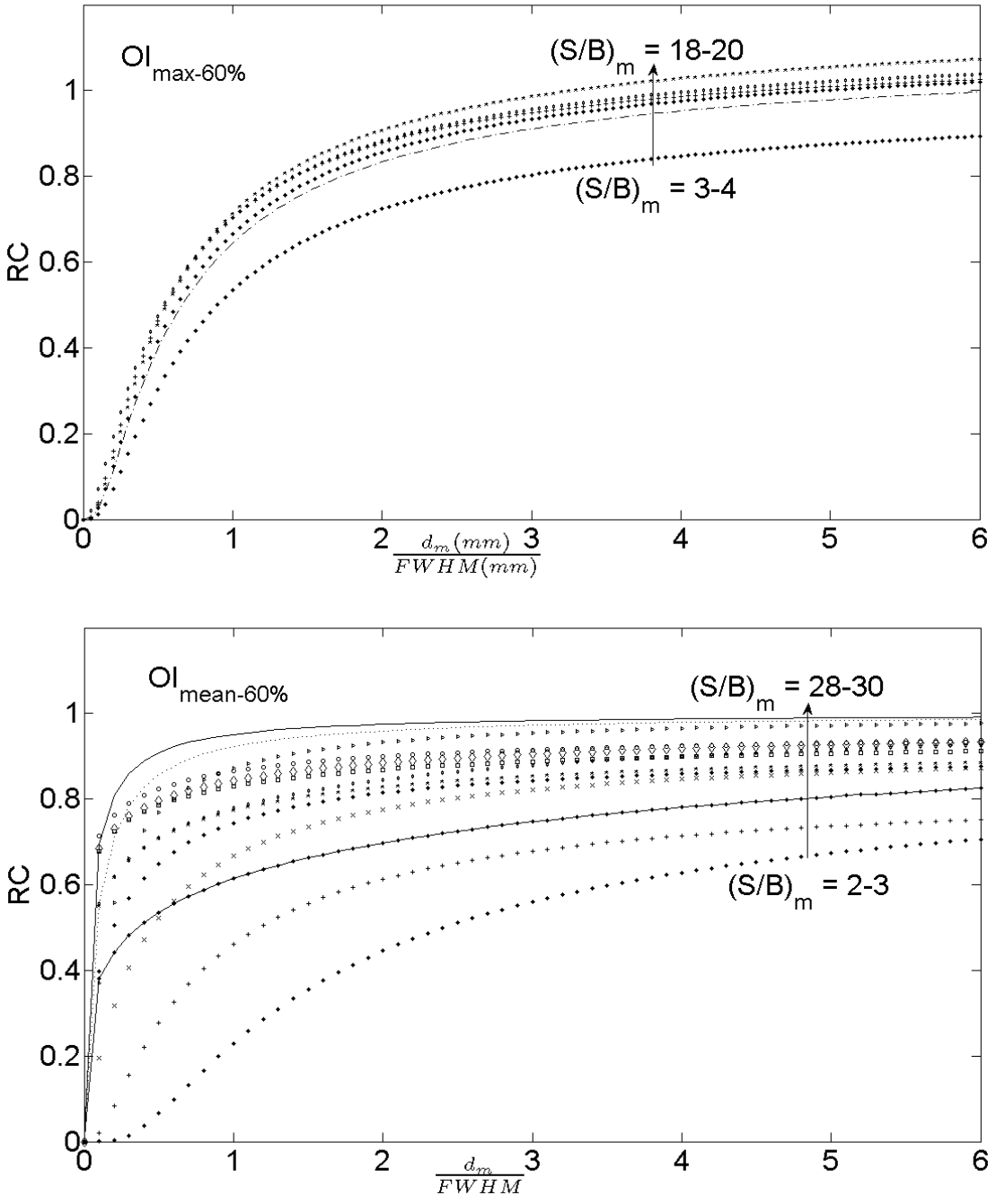

Figure 2.5: Set of RC curves for the OI $_{max-PET}$ and OI $_{mean-PET}$ measurement techniques with a 60% threshold

C_m was found to be greater than C_{GS} because of the high noise statistical fluctuations in the PET images. Since RC values greater than 1 produce additional underestimation of the radioactivity concentration as an effect of the PVE correction, we did not extract the RC curves for (S/B)m > 20.

For the measurement techniques using the mean C_m value, different set of RC curves were obtained, with $(S/B)_m$ from 2 to 30.

RC noise sensitiveness

The percentage difference of RC over the acquisition time (2.5, 5, 10, 15, 30 min), is more important for the techniques using the maximum value than the techniques using the mean value. The $OI_{mean-PET}$ techniques shows a grater noise sensitiveness compared with the $OD_{mean-PET}$ and $OD_{mean-CT}$ techniques.

However, as general results, we found that the percentage difference of RC over the acquisition time (2.5, 5, 10, 15, 30 min) is less than 10%, considering both the OD and the OI techniques, using maximum or mean uptake value.

This confirms that RC was found poorly sensitive to the noise level on the PET images for acquisition time from 30 min down to 2.5 min, proving the noise independency of the method to estimate RC: this guarantees the feasibility of our RC-based PVE correction method for clinical studies of acquisition time from 2.5 min (standard whole-body PET scan/bed) up to 30 min.

2.4.3 Accuracy of the PVE correction method

In order to evaluate the accuracy of the PVE correction method using the different measurements techniques, residual errors after PVE correction were evaluated as the percentage difference between the C_{GS} and PVE-corrected radioactivity concentration using anthropomorphic phantoms.

PVE correction was found poorly affected by the number of ROIs used to assess the background uptake: the percentage difference using one, two three or four ROIs was found lower than 10% in 80% for brain phantom acquisitions, 74% for thorax phantom acquisitions, and 87% for breast phantom acquisitions. In particular when four ROIs were used by two independent operators, similar results were found (CV=5.7%).

Table 2.5 shows, for each sphere of the anthropomorphic phantoms, the relative difference between C_{GS} and C_m before and after correction, obtained in independent experiments and averaged over different $(S/B)_m$

The results in Table 2.5 show that the techniques using the maximum of radioactivity concentration as measure of C_m (OD_{max-CT}, $OD_{max-PET}$, $OI_{max-PET}$) give a more precise estimate of the actual radioactivity concentration (C_{GS}) than the techniques using averaged radioactivity concentration, consistently with the results from the NEMA IQ phantom measurements and with the literature [48].

Considering the OD_{max-CT}, $OD_{max-PET}$ techniques, the definition of V_m on CT and PET images did not in any way influence the measurement of C_m, so the better definition of lesion volume on CT images did not improve significantly the quantification of radiotracer uptake.

It is clear that, even if this two techniques have a similar degree of accuracy with respect to the PVE correction, the OD_{max-CT} technique requires that the lesion is visible on CT images. In the case of phantom studies, the spheres simulating lesions are always visible on CT images, instead this can be critical for oncological PET/CT studies. In fact, notwithstanding the CT images were always studied in combination with the PET images to accurately localize the lesions, the lesion density, as it appeared on the CT images, is, in many cases, similar to the density of the surrounding tissues, making difficult to define lesions on CT images.

Table 2.5: ACCURACY OF THE PVE CORRECTION METHOD

	% $\frac{(C_m - C_{GS})}{C_{GS}}$ without PVE correction						
	d_{GS} (cm)	OD_{max-CT}	$OD_{max-PET}$	$OD_{mean-CT}$	$OD_{mean-PET}$	$OI_{max-PET}$	$OI_{mean-PET}$
Brain	9.8	0.57 ± 0.05	0.57 ± 0.05	0.68 ± 0.08	0.83 ± 0.08	0.57 ± 0.05	0.55 ± 0.05
	12.3	0.40 ± 0.03	0.40 ± 0.03	0.59 ± 0.06	0.72 ± 0.04	0.40 ± 0.03	0.43 ± 0.02
	15.6	0.26 ± 0.04	0.26 ± 0.04	0.50 ± 0.06	0.63 ± 0.05	0.26 ± 0.04	0.33 ± 0.04
Thorax	9.8	0.57 ± 0.08	0.57 ± 0.08	0.68 ± 0.03	0.74 ± 0.02	0.57 ± 0.08	0.58 ± 0.08
	12.3	0.36 ± 0.11	0.36 ± 0.11	0.53 ± 0.03	0.77 ± 0.02	0.36 ± 0.11	0.40 ± 0.05
	15.6	0.20 ± 0.03	0.20 ± 0.03	0.43 ± 0.02	0.56 ± 0.03	0.20 ± 0.03	0.30 ± 0.04
	25.8	0.18 ± 0.02	0.18 ± 0.02	0.31 ± 0.02	0.35 ± 0.01	0.18 ± 0.02	0.28 ± 0.01
	31.3	0.16 ± 0.01	0.16 ± 0.01	0.33 ± 0.02	0.37 ± 0.01	0.16 ± 0.01	0.27 ± 0.02
Breast	9.8	0.60 ± 0.01	0.60 ± 0.01	0.72 ± 0.04	0.81 ± 0.04	0.60 ± 0.01	0.60 ± 0.01
	12.3	0.39 ± 0.01	0.39 ± 0.01	0.45 ± 0.03	0.52 ± 0.04	0.39 ± 0.01	0.43 ± 0.05
	15.6	0.16 ± 0.12	0.16 ± 0.12	0.48 ± 0.17	0.57 ± 0.05	0.16 ± 0.12	0.23 ± 0.03
	25.8	0.12 ± 0.08	0.12 ± 0.08	0.53 ± 0.05	0.30 ± 0.06	0.12 ± 0.08	0.27 ± 0.04
	31.3	0.12 ± 0.08	0.12 ± 0.08	0.46 ± 0.05	0.29 ± 0.05	0.12 ± 0.08	0.23 ± 0.05
	% $\frac{(C_m - C_{GS})}{C_{GS}}$ with PVE correction						
	Diameter (cm)	OD_{max-CT}	$OD_{max-PET}$	$OD_{mean-CT}$	$OD_{mean-PET}$	$OI_{max-PET}$	$OI_{mean-PET}$
Brain	9.8	0.32 ± 0.10	0.28 ± 0.06	0.27 ± 0.01	0.26 ± 0.10	0.29 ± 0.05	0.24 ± 0.05
	12.3	0.22 ± 0.03	0.13 ± 0.10	0.17 ± 0.05	0.29 ± 0.04	0.11 ± 0.03	0.11 ± 0.02
	15.6	0.18 ± 0.02	0.10 ± 0.08	-0.006 ± 0.11	0.28 ± 0.10	0.05 ± 0.04	0.05 ± 0.04
Thorax	9.8	0.23 ± 0.16	0.23 ± 0.12	0.29 ± 0.26	0.45 ± 0.09	0.28 ± 0.11	0.27 ± 0.01
	12.3	0.17 ± 0.07	0.02 ± 0.10	0.05 ± 0.03	0.28 ± 0.11	0.06 ± 0.14	0.07 ± 0.04
	15.6	0.10 ± 0.09	-0.04 ± 0.05	0.03 ± 0.08	0.25 ± 0.19	-0.02 ± 0.08	0.04 ± 0.05
	25.8	0.01 ± 0.04	0.01 ± 0.03	-0.08 ± 0.07	-0.13 ± 0.18	0.02 ± 0.04	-0.03 ± 0.10
	31.3	0.08 ± 0.01	0.09 ± 0.02	0.11 ± 0.07	-0.04 ± 0.05	0.05 ± 0.01	0.05 ± 0.03
Breast	9.8	0.27 ± 0.10	0.25 ± 0.07	0.28 ± 0.04	0.31 ± 0.12	0.30 ± 0.07	0.26 ± 0.12
	12.3	0.15 ± 0.05	0.07 ± 0.02	-0.01 ± 0.07	0.27 ± 0.19	0.14 ± 0.01	0.13 ± 0.06
	15.6	0.05 ± 0.05	-0.02 ± 0.05	0.09 ± 0.10	0.26 ± 0.02	-0.02 ± 0.01	0.002 ± 0.002
	25.8	0.07 ± 0.07	0.02 ± 0.14	-0.05 ± 0.07	-0.01 ± 0.02	-0.01 ± 0.12	0.09 ± 0.03
	31.3	0.07 ± 0.02	0.08 ± 0.09	-0.01 ± 0.09	0.05 ± 0.05	0.03 ± 0.09	0.10 ± 0.01

Considering the $OD_{mean-CT}$ and the $OD_{mean-PET}$ techniques, it was found that the measure of C_m was more accurate when lesion volume is defined on CT images rather than on PET images. Also the PVE correction was found more effective for the $OD_{mean-CT}$ technique than for $OD_{mean-PET}$ technique. In case of the $OD_{mean-CT}$ technique, the possibility to define lesion on CT images is required as for the OD_{max-CT} technique. Considering the OI techniques, the $OI_{max-PET}$ and the $OI_{mean-PET}$ techniques show similar behavior when PVE correction is applied, even if the residual error is always smaller for the $OI_{mean-PET}$ technique. Results showing a poor dependency of the background measurements on PVE correction, confirm the independency of OI techniques from operators. Some negative values in the relative differences were found after PVE correction as the result of an overcorrection for PVE. For all the measurement techniques, there was a drop in accuracy for lesions with d < 1cm, compatible with the severe errors in volume estimation reported for a tumor volume < 2 mL [48, 49]. In this case a deconvolution approach could be investigated to improve the accuracy of the PVE correction.

The performance of the developed PVE correction method, considering all the measurement techniques, is summarized in Table 2.6, in terms of accuracy, operator dependency and applicability.

Table 2.6: PERFORMANCE OF THE PVE CORRECTION METHOD

Techniques using the maximum uptake

OD_{max-CT}	$OD_{max-PET}$	$OI_{max-PET}$
Operator dependent technique	Operator dependent technique	Operator independent technique
Not always applicable: $(L/B)_m$ <20, CT volume available	Not always applicable $(L/B)_m$ <20	Not always applicable $(L/B)_m$ <20
Accuracy>68% (d<1cm) Accuracy>78%(d>1cm)	Accuracy>72% (d<1cm) Accuracy>87%(d>1cm)	Accuracy>70% (d<1cm) Accuracy>86%(d>1cm)

Techniques using the mean radiotracer uptake

$OD_{mean-CT}$	$OD_{mean-PET}$	$OI_{mean-PET}$
Operator dependent technique	Operator dependent technique	Operator independent technique
Not always applicable: CT volume available	Always applicable	Always applicable
Accuracy>71% (d<1cm) Accuracy>83%(d>1cm)	Accuracy>55% (d<1cm) Accuracy>71%(d>1cm)	Accuracy>73% (d<1cm) Accuracy>87%(d>1cm)

2.4.4 Clinical applicability of the PVE correction method

Optimized measurement technique for patient studies analysis

Following the results for the accuracy, the applicability and the advantages of the PVE correction method with respect to the different measurement techniques, the quantification of oncological PET/CT studies for both follow up and breast cancer patients was performed using the $OI_{mean-PET}$ technique.

This technique combines the advantages of a full independent measurement technique with a lower dependency on noise and the better accuracy for RC-based PVE correction method.

Clinical feasibility

For both the follow up (basal and follow up PET/CT studies) and breast cancer patients, 92% of the lesions were found to be spherical, and 85% had uniform radioactive uptake.

V_m was always definable on PET images. In particular, the measured V_m and $(L/B)_m$ of the considered lesions were in the range of experimental RC curves (the sphere-equivalent d_m from 0.4 to 4.2 and $(L/B)_m$ was from 1.6 to 35; background mean CV = 6.28 $\pm$ 3.00; background CV range: 1.6-10.4).

These results confirm the feasibility of the developed PVE correction approach to real PET/CT oncological studies for the $OI_{mean-PET}$ technique.

Follow up patients

Concerning PET/CT studies of follow up patients, PVE correction was found to modify SUV_{BW} and δSUV_{BW} for all the lesions, as confirmed by a statistical analysis (paired t-test) that proved that the distributions of SUV_{BW} and δSUV_{BW} were statistically different before and after PVE correction ($p<0.01$), underlining the significance of the correction. Tables 2.7 and 2.8 summarize the main results on the clinical feasibility of the PVE correction approach, and the quantitative results for the application of PVE correction using the designed $OI_{mean-PET}$ technique.

After PVE correction, SUV_{BW} was found to be increased by more than 25% in 52% of lesions, and PVE correction reduces δSUV_{BW} in 63% of lesions from 5% to 65%.

When δSUV_{BW} increased, an increase of more than 25% was found in 48% of lesions. This is important considering that, according to 1999 EORTC recommendations [50], SUV_{BW} variations of more than 25%, as an effect of the PVE correction, can change the classification of lesion's metabolic evaluation.

An exhaustive evaluation of the effects of PVE correction on diagnostic confidence is beyond the purpose of this work, and would, in any case, require a larger set of patient studies. However, our results on the follow up studies suggest that PVE correction must be applied if SUV_{BW} is used to support diagnosis and/or to classify lesion metabolic evaluation.

As a representative example, the 1999 EORTC classification of tumor response for patient n. 1, presenting three lesions (lesions n° 1, 2, 3, respectively in Table 2.7) as metastases from ovarian cancer at the basal study, and the same three lesions at the follow up study (no new metastasis). Before PVE correction, the evaluation of lesions n.1 and n.2 classifies the tumor response as *partial metabolic response*, while the evaluation of lesion n.3 indicates *stable metabolic disease* (δSUV_{BW}, which is at a limit of 25%). After PVE correction, the evaluation of the three lesions classified the tumor response as *partial metabolic response* with increased diagnostic confidence (corrected δSUV_{BW} « -25%).

Breast cancer patients

Table 2.9 shows the results for the quantification of the breast cancer patients.

Considering breast cancer patients, the PVE correction was found to modify SUV_{BW} up to 47%. As general result, PVE-corrected SUV_{BW} is statistically different from SUV_{BW} ($p< 0.01$) and, in 25% of lesions, PVE correction made SUV_{BW} to reach the malignancy threshold of 2.5 gr/cc for lesions, considered benign before PVE correction for almost three lesions.

Table 2.7: FOLLOW UP PATIENTS QUANTIFICATION RESULTS - BASAL PET/CT STUDY

	Basal PET/CT oncological study					
Lesion n°	Roundness	Uniformity	d_m (cm)	$(L/B)_m$	SUV_{BW} (g/cc)	PVE-corrected SUV_{BW} (g/cc)
1	Y	Y	0.62	12.3	9.5	13.6
2	Y	Y	0.98	15.1	14.2	17.4
3	Y	Y	0.79	16.3	14.0	17.9
4	Y	Y	1.45	2.3	3.8	5.3
5	Y	Y	0.38	11.7	18	30.6
6	Y	Y	0.8	5.6	13.8	19.2
7	Y	Y	1.09	2.1	3.2	5.0
8	Y	Y	0.56	8.1	7.2	10.2
9	Y	Y	1.5	1.9	4.1	8.4
10	Y	Y	1.1	6.1	8.1	12.7
11	N	Y	1.8	4.4	3.7	4.3
12	Y	Y	1.2	4.9	8.4	10.5
13	Y	Y	0.9	5.6	6.1	8.2
14	Y	Y	1.2	1.9	2.9	6.6
15	N	Y	2.2	8.1	14.4	15.9
16	Y	Y	2.0	8.9	8.1	9.1
17	Y	Y	1.0	6.0	4.8	6.3
18	Y	N	3.6	11.4	23.1	24.7
19	Y	Y	1.4	4.1	4.2	5.0
20	Y	Y	1.4	5.9	6.9	8.5
21	Y	Y	0.7	3.5	5.3	7.6
22	Y	Y	1.4	1.6	5.3	7.4
23	Y	Y	1.4	3.6	5.9	7.1
24	Y	Y	1.5	4.1	6.4	7.6

2.5 Conclusion and Discussion

The purpose of the first part of phD work was the development and the validation of a method to *in vivo* quantify radiotracer uptake in PET/CT oncological studies. This implied the development and validation of a method for PVE correction in PET. A RC-based PVE correction approach was designed and proved accurate, feasible and easy to be implemented in a clinical environment for real PET/CT whole-body oncological studies.

2.5.1 Measurement techniques

In order to measure lesion uptake and lesion volume on PET/CT images both OD and OI techniques were developed. Results of our assessment showed different performance for the measurement techniques, consistently with other results [4, 15, 48].

The techniques that measure V_m on CT images (OD_{max-CT} and $OD_{mean-CT}$) were found limited because:

- oncological lesions are not always clearly visible on CT images, (e.g. lesions in soft tissue)
- when visible, lesion volume on CT images could present differences with respect to lesion volume on PET images [31]

Table 2.8: FOLLOW UP PATIENTS QUANTIFICATION RESULTS - FOLLOW UP PET/CT STUDY

	Follow up PET/CT oncological study					
Lesion n°	Roundness	Uniformity	d_m (cm)	$(L/B)_m$	SUV_{BW} (g/cc)	PVE-corrected SUV_{BW} (g/cc)
1	Y	Y	0.97	8.8	7.0	8.6
2	Y	Y	1.04	9.1	7.6	9.7
3	Y	N	1.16	5.3	10.6	13.0
4	Y	Y	1.3	2.1	3.3	4.7
5	Y	Y	1.12	11.5	15.5	19.1
6	Y	Y	1.3	5.8	8.1	10.0
7	Y	Y	1.5	2.7	4.6	6.4
8	Y	Y	1.0	9.2	8.2	10.1
9	Y	N	2.4	4.3	5.7	7.6
10	Y	N	3.7	6.2	3.5	8.2
11	Y	Y	2.6	5.2	4.4	4.9
12	Y	Y	1.5	6.9	7.2	8.2
13	Y	Y	1.1	4.8	4.4	5.6
14	Y	Y	0.6	2.3	4.9	9.7
15	N	Y	1.4	2.3	2.9	4.0
16	Y	N	1.8	5.8	3.5	4.1
17	Y	Y	1.1	3.5	2.0	2.5
18	Y	N	5.4	5.4	8.7	9.2
19	Y	N	2.1	5.4	5.4	6.2
20	Y	N	2.2	3.6	3.0	3.4
21	Y	Y	1.3	2.0	2.1	3.1
22	Y	Y	1.2	1.8	4.8	7.1
23	Y	Y	1.2	3.5	3.4	4.2
24	Y	Y	1.7	2.4	2.8	3.6

- CT volume calculation is sensitive to inter-operator measurement differences, presenting problems of reproducibility and stability.

On the other hand V_m can be always defined on PET images. In this case, measuring C_m as the maximum radioactivity concentration, C_m values are sensitive to PET image noise. When C_m is averaged over V_m, if V_m is manually measured, C_m values are highly variable and fully dependent from the operator calculations on PET images. However if V_m is measured by an automatic threshold technique, the operator-dependency is reduced to the only choice of the position of the four background ROIs. In fact our results show a variability < 10% in the background definition performed by three different operators. Different thresholds were explored and the optimized threshold (60%) allows the optimal approximation of V_m to the actual volume.

2.5.2 PVE correction method

With the purpose of clinical feasibility, a PVE correction approach based on information from patient PET/CT oncological images (intrinsically affected by PVE) was developed. For this reason, RC curves were obtained as a function of PET/CT measured V_m and PET/CT measured $(S/B)_m$: in this way, a full consistency between the direct procedure to obtain RCs from hot spheres and the inverse procedure to apply 1/RC factor for PVE correction of hot lesions was obtained.

Table 2.9: BREAST CANCER PATIENTS QUANTIFICATION RESULTS

	Breast cancer patient PET/CT oncological study					
Lesion n°	Roundness	Uniformity	d_m (cm)	$(L/B)_m$	SUV_{BW} (g/cc)	PVE-corrected SUV_{BW} (g/cc)
1	Y	Y	0.5	14.3	2.6	3
2	Y	Y	4.2	4.7	4.3	5.6
3	Y	Y	0.4	4.7	1.4	2.0
4	Y	Y	1.6	34.9	8.9	9.5
5	Y	Y	1.1	11.0	5.2	6.3
6	N	Y	1.0	5.3	1.8	2.4
7	Y	Y	3.2	7.2	4.8	5.8
8	N	N	2.2	10.9	3.6	4.3
9	Y	Y	3.1	10.2	3.1	4.0
10	Y	Y	1.1	13.1	4.5	5.1
11	Y	Y	2.0	4.4	1.7	2.5
12	Y	Y	1.8	5.0	1.7	2.3

Approximations, constraints, advantages and disadvantages

The developed PVE correction method allows a quantification of PET/CT oncological studies at a region level (within lesions): no correction of the whole images can be achieved and PVE correction has to be applied separately to different lesions on the PET images.

Furthermore, RC curves and validation measurements were obtained for a specific PET/CT system and by the use of hot spheres miming spherical oncological lesions with an uniform uptake of ^{18}F-FDG. Then, our PVE correction can be confidently applied to PET/CT patient studies under some requirements:

- the same reconstruction algorithm used for the image reconstruction of the NEMA IQ phantom has to be applied to patient images.
- lesions must shown glucose hyper-metabolism: the hypometabolic lesions (e.g. low-grade tumour in the cerebral white matter) can be corrected using other PVE correction methods [18, 51].
- lesions must have a spherical shape: some results from Monte Carlo simulations showed that RC-based PVE correction can be used in non-spherical objects [48, 52]; however, for non-spherical lesions, the developed PVE correction approach should be used carefully and it needs optimization as well as validation.
- lesions must have an uniform radiotracer uptake: as for non-spherical lesion, particular care must be used for the application of the developed PVE correction approach to heterogeneous lesions. A recent work focused on the impact of PVE correction on tumor heterogeneity suggests, in this case, the use of local image deconvolution approach with expectation maximization and spatially variant point spread function [53].

From our results on oncological patients, acquired on the same PET/CT system used for RC estimation, 100% of patients presented lesions with glucose hyper-metabolism in different body regions, and the last two requirements were satisfied by a large percentage of lesions (92% for roundness and 85% for uniformity).

RC values were obtained at a fixed distance (5.5 cm) from the center of axial field. The different location of the validation spheres and of the patient lesions has been compensated by

normalizing the PET measured object size to the PET image spatial resolution (FWHM) at the sphere/lesion location.

V_m correction was not considered in this approach, requiring several segmentation techniques [54] or the availability (or the competence for the development) of complex image processing tools.

The developed PVE correction method has the main advantage be easy to be implemented in a nuclear medicine environment, requiring the only use of standard phantoms and simple measurement protocols, without developing dedicated software incorporated during or after the reconstruction process.

Potentials

RC values obtained in this work to perform the PVE correction were measured using a dedicated PET/CT system and with a specific reconstruction method. Despite this, the considered PVE correction method can be applied a posteriori to other reconstruction methods and to other PET/CT system, on condition that the same PET/CT system is used to patient and phantom studies, that the same reconstruction algorithm is applied both to NEMA phantom images (for the estimation of RC) and to patient images (for the PVE correction) and that the accuracy of PVE correction is confirmed.

The considered PVE correction approach can be applied also to PET radiotracers different from ^{18}F-FDG with the same limitations (e.g. hypometabolic, spherical, and homogeneous radioactive lesions). Obviously, since RC are both radiotracer-dependent, new PET/CT measurements with NEMA IQ phantom are required to obtain proper RC factors.

Chapter 3

Approaches to integration of PET/CT data, hystological parameters and proteomic data

3.1 Introduction

Molecular imaging techniques are, in large part, devoted to study oncological pathologies. *Ex vivo* analysis of cancer tissue allows to characterize tumor tissue and tumor invasiveness, as well as to carry out the surgical intervention [55, 56]; *ex vivo* proteogenomic analysis are devoted to find molecular features in terms of genes and proteins selectively expressed in cancer cells [57, 58, 59, 60, 61, 62]; *in vivo* molecular techniques such as CT or PET/CT studies allow to visualize cancer anatomical and functional traits [63].

In recent years various efforts are spent to connect the information obtained by both *in vivo* and *ex vivo* molecular techniques: the challenge is that the exchange of information between *in vivo* and *ex vivo* molecular imaging data will allow a more accurate diagnostic approach, simplifying the comprehension of the multi-factorial origin of some diseases and will allow to personalized therapy and cure protocols.

The integration of *in vivo* with *ex vivo* molecular imaging data is one of the more ambitious challenge in the approach of the *personalized medicine*: the correlation of *in vivo* biomarkers with *ex vivo* histopathological, or proteogenomic data can be crucial for disease staging or cure monitoring by clinical routine procedures, as, in the case of oncological disease, for tumour aggressiveness or therapy response.

In many oncological studies, indexes of glucose metabolism, as Standard Uptake Value (SUV) [6], measured *in vivo* and non invasively by PET and ^{18}F-FDG, have been already studied in association with *ex vivo* histopathological findings [12, 26, 34, 38, 39, 64, 65, 66]. Encouraging results have come more recently from two published studies on oncological patients devoted to the integration of *ex vivo* genomic and *in vivo* PET data [1, 2] or *in vivo* CT data [3]. Both studies have shown that quantitative or semi-quantitative parameters obtained from *in vivo* molecular imaging (anatomical or functional) systematically correlate with a big amount of information relative to lesion gene expression profiles, opening a new role to *in vivo* molecular imaging in the current approach of integrated molecular medicine.

Data integration requires the development of new methods and infrastructures for an efficient data management, from their collection and archiving, with the final goal to find correlations among *in vivo* (PET/CT studies) and *ex vivo* data (proteomic and hystological data) by innovative statistical models, in order to personalize the diagnostic and therapeutic treatment of patients.

The aim of the second part of this phD project was to develop methods and infrastructures for the integration of *in vivo* and *ex vivo* molecular imaging techniques in oncology, and their application to a specific case of a population of breast cancer patients.

The approach of integration data analysis consists into the development and optimization of:

- integrated protocols for single-patient *in vivo* and *ex vivo* data collection;
- methods for the extraction of biomarkers for prognosis/diagnosis from *in vivo* molecular imaging
- innovative infrastructures and data analysis methods including databases and statistical techniques for data correlations.

3.2 Materials and methods

3.2.1 Data collection

An integrated protocol for the collection of *in vivo* and *ex vivo* data was conceived and implemented for a representative population of patients with breast cancer, requiring a strong collaboration among different specialists (surgeons, nuclear physicians, pathologist, biologists).

The protocol included

1. the recruitment of patients and collection of clinical data
2. the collection of PET/CT patient images
3. the collection of hystopathological data after surgery
4. the collection of proteomic data after surgery

The protocol schedule, developed at IRCCS San Raffaele, consisted of the enlistment of adult females with breast cancer with tumor mass > 1cm that were designed for surgical intervention without performing any treatment before surgery. Patients had to provide the informed consensus to donate biological samples collected during surgery.

The specialist in senology collected all the patient information that can be involved as prognostic factor for breast cancer development as age, genetics (cancer family history), menopausal status, years menstruating, number of pregnancy, breastfeeding, obesity, and exogenous factors (hormone replacement therapy, use of oral contraceptive pills, alcohol consumption, smoking).

Eligible patients undergo a total-body PET/CT exam before surgery. The nuclear physician collected all the information about the PET/CT exam needed for PET/CT quantification (administered and residual activity, schedule time, patient weight and height).

Following the PET/CT exam, the patient underwent the surgery intervention and biological samples, collected during the surgery, are despatched at the Pathological Anatomy Unit for the subsequent hystopathological analysis. The ordinary clinical hystopathological analysis allows to classify tumors according to the WHO guidelines [67], and consist into the evaluation of hystological type, hystological grade, hormone receptor status, proliferation indices, and mitotic counts.

A portion of cancer tissue as well as normal breast tissue was stored for proteomic analysis, performed through 2D-Difference Gel Electrophoresis (2D-DIGE) and mass spectrometry, in order to evaluate the proteins differentially expressed in breast cancer tissue with respect to breast normal tissue.

3.2.2 Infrastructure for data storage and data analysis

Storing and saving of the patient data was worked out so that the procedure was found effective, fast and easy to perform for all the involved specialists: a Virtual Lab (VL), connecting all the involved unit, was developed for the integration of *in vivo* and *ex vivo* data of individual patients obtained from the different diagnostic molecular imaging modalities. The laboratory virtually connected, through internet and a dedicated infrastructure, different hospital units and research laboratories.

The web interface of the VL has been developed in PHP language and designed to allow the different users to upload the patient data into a MySQL database, from their proper personal computer. The developed database was optimized for storing and analysis of large amount of data from different modalities (e.g. numerical from PET/CT and histopathology, logical from histopathology, proteomics and genomics).

Every patient was identified and anonymized by a protocol-dependent identification number to warrant the patient privacy. Every data was categorized (e.g. qualitative-nominal/qualitative-ordered, quantitative-discrete/quantitative-continuous), standardized and archived in standard formats (e.g. DICOM).

The data repository has been implemented on a dedicated worker node linked to the virtual network of the laboratory and to internet. The worker node was the touchscreen server workstation in which cOuch was developed (see Appendix A). cOuch was linked to the database for data statistical analysis developing proper data integration tools.

3.2.3 Statistical data analysis

The first step for the development of statistical tools consisted in the evaluation of the approach to be considered to integrate the heterogeneity of data (clinical, proteomic, histological and functional data) collected for each patients.

Some data are intrinsically continuous (SUV, hormone receptor, protein expression level, ...), other parameters are categorical (histological type, histological grade,...).

SUV_{BW} is an intrinsically continuous variable, although for some kind of statistical analysis, patients could be stratified on the basis of a SUV threshold or in groups of negative/ positive with respect to the ^{18}F-FDG uptake.

Considering the results of literature, histological data were treated as dichotomous and categorical, also following the different kind of developed statistical analysis. In particular, hormone receptor (ER, PgR), monocolonal antibody Mib-1, c-erbB-2 oncogene were treated as positive or negative using a defined threshold [68, 69, 70]. On the other hand hystological grade, assessed by the pTNM classification, [71, 72], was considered as an ordinal variable. Hystological type was classified as an ordinal variable on the basis of epidemiologic incidence [73].

The protein expression levels are continuous data, expressed as relative abundance of the signal peak of each protein in cancer tissue with respect to the normal tissue. In order to avoid the problems due to the inaccuracies of quantitative proteomic data, various type of analysis were implemented considering the original data or their reduction to dichotomous data (up/down-regulated proteins).

Several bi-variate statistical tests (e.g. Mann-Whitney and Kruskal-Wallis correlation tests) have been implemented in cOuch to assay the relationship of quantitative PET parameters (e.g. Standard Uptake Value, SUV, functional lesion volume, anatomical lesion volume) with histological indexes (e.g. ER, PgR) and up/down regulated proteins (e.g. Adenosine kinase, Beta-actin).

Mann-Whitney test was implemented as one-to-one test to assess the dependency of PET quantitative parameters from the dichotomous parameters. This test performs a comparison between the two distributions of the PET parameter corresponding to the two different values of the binary

parameter, testing the null-hypothesis that the two independent samples come from distributions with equal medians. Rejecting the null-hypothesis means that PET parameter is dependent from the dichotomous parameter.

The Kruskal-Wallis test is a generalization of the Mann-Whitney test used for categorical parameters and it was implemented as one-to-one test assessing the dependency of PET parameters from categorical variables, such as hystological grade and istotype.

Moreover, a SUV-based dynamic threshold clustering algorithm was implemented to evaluate the correlation of SUV versus different groups of parameters. In this approach the SUV is treated as binary variable on the basis of dynamic threshold. The starting threshold was fixed to 2.5 g/cc, the cut-off used in literature to distinguish benign and malignant pathologies.

A dedicated interface, developed in cOuch, allow data recovery from the database and their use to perform statistical tests.

Validation of the implemented statistical tests was performed using a data set of simulated data, obtained using Cholesky decomposition [74]. Given a correlation matrix, the Cholesky matrix is a square root matrix that multiplied with itself gives the original correlation matrix. To obtain the correlated random deviates given a correlation matrix A, it is sufficient to operate the vector of random variables with the Cholesky matrix, generated by A matrix.

3.3 Results

3.3.1 Data collection

The innovative aspect of the integrated developed protocol is that it involves different hospital units and research labs, requiring an high grade of cooperation as well as an efficient organization.

The protocol was approved by the Institutional Review Board of the IRCCS San Raffaele for twenty patients.

Patient recruitment was found quite efficient. In fact only one patient was excluded because, following the PET/CT exam, the specialist in senology decided to perform chemotherapy rather than the surgical intervention. However in four patient the pathologist did not succeed to keep a part of cancer tissue for the subsequent proteomic analysis, due to the specimen dimension, all used for clinical hystological analysis following surgical intervention. Finally, two patients were excluded from the protocol because, after the PET/CT exam, other primitive oncological pathologies (in one case a lung cancer, in the other case a sarcoma) were diagnosed and patients followed other therapies. For this reasons, it was necessary to leave out some of the selected patients from the protocol, and so it was necessary to extend the protocol to other patients and a total number of 30 patients were enrolled in the protocol (see Table 3.1).

Patients data collection was found efficient: no loss of patients data or specimens between units was founded for all the enrolled patients.

Patient data flux required long time. In fact, from the starting recruitment performed by the specialist in senology, patients were immediately directed to nuclear medicine department. After the PET/CT exam, surgical intervention was performed after a high variable time period (from 1 week to two month), due to the clinical schedule of the senology unit. Hystological analysis of the patient specimens were required three days after surgical intervention , while for the proteomic analysis it was decided to wait the conclusion of the extended protocol in order to avoid loss of reproducibility due to difference in gel treatment and analysis. It is forecast that the proteomic analysis will require, at least, one month.

Table 3.1: BREAST CANCER PATIENTS

Patient number	Age (y)	Notes
1	55	
2	45	
3	70	
4	65	
5	40	
6	38	
7	75	
8	37	No sufficient specimens for proteomic analysis
9	69	
10	55	No sufficient specimens for proteomic analysis
11	71	
12	80	
13	48	
14	60	
15	68	Lung cancer diagnosis after PET/CT exam
16	59	Sarcoma diagnosis after PET/CT exam
17	41	Chemotherapy performed before surgery
18	47	No sufficient specimens for proteomic analysis
19	37	No sufficient specimens for proteomic analysis
20	45	
21	58	
22	41	
23	64	
24	74	
25	67	No sufficient specimens for proteomic analysis
26	51	
27	70	
28	36	
29	70	No sufficient specimens for proteomic analysis
30	74	

3.3.2 Infrastructure for data storage and data analysis

The developed virtual lab was implemented so that, after authentication and authorization, each user can access at a dedicated window guiding in the patient data upload, selectively accessing to pages authorized according to the professional role in the lab.

Specifically, the lab web site consists of a page for the login and dedicated pages for data submission (clinical, histological, PET/CT and proteomic data). Figure 3.1 shows the authentication window of the developed VL.

Figure 3.2 shows the window for clinical data submission that has to be filled by the specialist in senology.

Figure 3.3 shows the window for PET/CT data submission that has to be filled by the nuclear physician. The database was developed to store the PET/CT data in DICOM format, as well as the quantitative numerical data obtained from the image analysis performed by cOuch software.

Figure 3.4 shows the window for hystological data submission that has to be filled by the

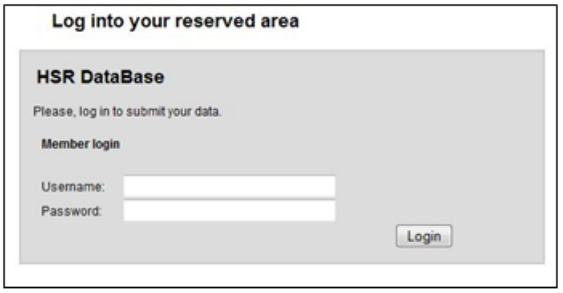

Figure 3.1: VL authentication window

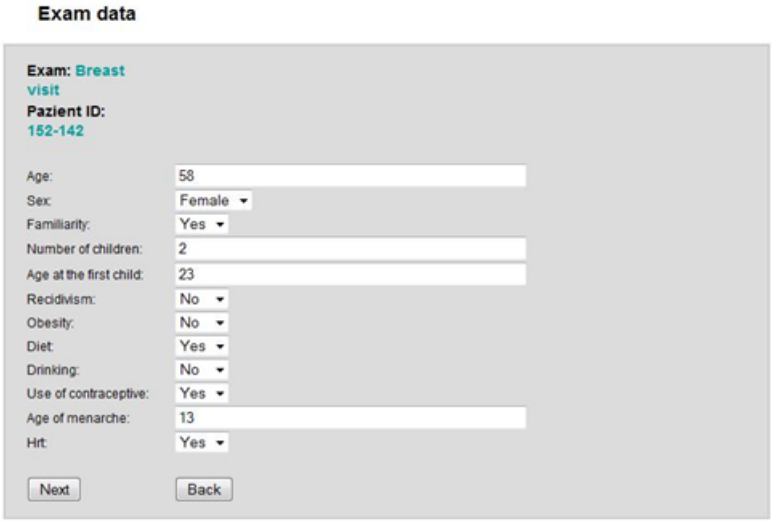

Figure 3.2: VL clinical data submission window

pathologist.

Figure 3.5 shows the window for proteomic data submission.

Biologists have to flag the proteins differentially expressed in cancer breast in a predetermined list [58, 59, 60, 61, 62], then have to insert if the proteins is found up or down regulated and the p-value obtained by the 2D-DIGE analysis.

The GUI of the VL was found user-friendly by all users.

The implemented infrastructure did not show any conflicts in data submission and recovery. No data loss or corruption were found and the VL resulted efficient both to store data and to use collected data in order to perform statistical analysis.

3.3.3 Statistical data analysis

Considering the case one-to-one test validation, the approach that was used to simulate correlated data using Cholesky matrix consisted in three passages. First, two vectors (20x1) of random variables were simulated using random number generators implemented in MATLAB; second, the correlation matrix for these variables was obtained and the Cholesky factorization was calculated; third, the Cholesky matrix was used to find two correlated random variables operating the created vectors of random variables for the Cholesky matrix.

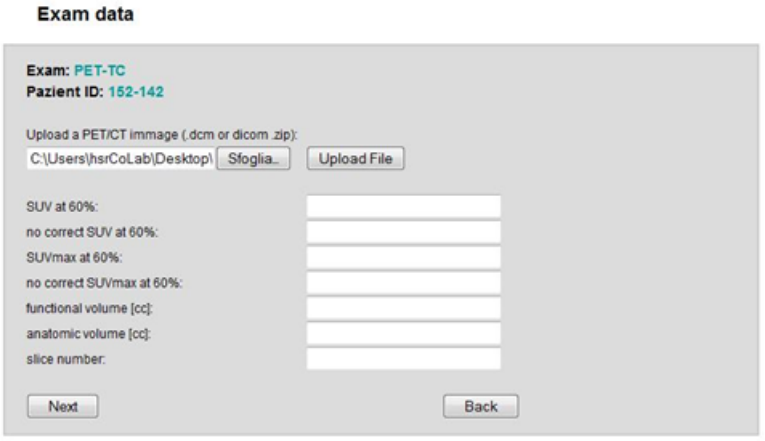

Figure 3.3: VL clinical data submission window

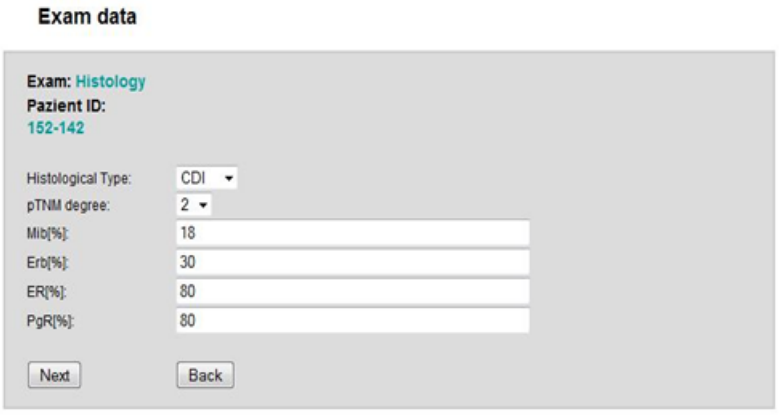

Figure 3.4: VL hystological data submission window

Using simulated data the implemented Mann-Whitney and Kruskal-Wallis tests were validated obtaining always correlated data ($p \ll 0.001$).

The validation of the multi-clustering approach was performed using a simulated data set of more thn two variables using the same Cholesky matrix approach already described, but it is clear that this procedure allows to validate only the implementation of the algorithm without giving any information about the behavior of the algorithm on the experimental data.

3.4 Conclusions

The purpose of the second part of this phD work was to study methods and infrastructures for the integration of clinical, hystopathological, protogenomic and PET/CT imaging data.

A dedicated integration protocol was developed for breast cancer patient and data flux and collection was found quite effiient, requiring the cooperation of the different involved specialists.

The proper developed infrastructure was found optimal for storage of patient data and for data recovery for subsequent statistical analysis.

Mann Whitney and Kruskal Wallis tests, developed for the assessment of the one-to-one relationships between SUV and other parameters, were used in other previous work [39] and were

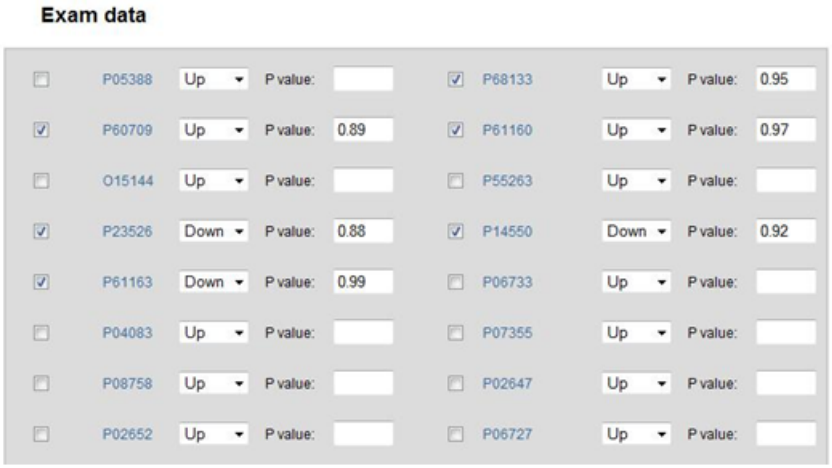

Figure 3.5: VL proteomic data submission window

found suitable for statistical analysis. Multi-clustering algorithm, developed for multivariate correlation test, has to be evaluated when applied to real oncological patient data.

The end of the protocol, with the collection of the entire breast cancer patient data set, will allows to obtain statistically significant results for the correlation of clinical, hystopathological, proteogenomic and PET/CT imaging data in the case of breast cancer patients.

Future studies have to be devoted to a more complete and general approach to multivariate tests considering all the involved patient parameters.

Appendix A

cOuch - Correlative and Collaborative Touch System

cOuch (Correlative and Collaborative Touch System) software is a standalone medical image viewer and image processing software tool used to display, process, archive, and communicate PET/CT images for the detection and characterization of several oncological pathologies. The software contains statistical tools for correlation analysis between PET/CT quantitative parameters and other patient data (proteomic data, hystopathological parameters, clinical data).

The software, developed as collaborative, interactive and multi-modality image tool, avoiding the use of keyboard or mouse, has been designed to provide a user-friendly and flexible way to images, and perform essential operations on them.

The software allows different operations:

- storing of patient data and patient exam data.
- fast and ergonomic access to PET/CT whole-body images: high-definition visualization of PET, CT and fused PET/CT images, with the management of different color tables
- easy manipulation of windows and buttons as well as of graphical objects and optimal scroll/pan/zoom of images.
- easy and immediate drawing of region of interest (ROI) on the images by a combination of manual/stylus control, following different developed ROI definitions.
- accurate calculation of lesion metabolic uptake, accounting for PVE (RC-base PVE correction [75])
- film preparation with the possibility to include text and annotations for collaborative purposes, free-hand medical reporting with digitally signature.
- statistical correlation tools

A.1 Architecture design

Couch is developed in MATLAB R2008a, matrix oriented programming environment, because it provides facile access to complex calculations and allow an easy code manipulation. Image Processing Toolbox, Statistic Toolbox and Curve Fitting Toolbox were used within the software algorithm. *Ad hoc* utilities were implemented with Java languages and therefore requires an appropriate Java Runtime Environment (JRE 1.6) to be executed.

A.2 Hardware design

The software run under Windows and has been implemented into the Desktop PC HP TouchSmart IQ820 which is equipped with a 25.5-inch touch screen, a 1920 x 1200 pixels resolution with a Intel processor Core^{TM}2 Duo P7450, 4 Giga byte RAM. Graphical acceleration is provided by a NVIDIA GeForce^{TM} 9600M GS HD graphic card, with 512 MB (until 2303 MB total memory) dedicated memory. The native operating system is Windows Vista Home Premium with Windows Media Center (64-bit). Neverthless it's possible to use COuch software also with another hardware (touchscreen or not touchscreen) but as a Matlab and Java application, the memory footprint of software is relatively big: the installed RAM should be minimally 1GB, 2 GB and above is recommended.

A.3 cOuch general functionality

The software cOuch provides access and analysis of the PET/CT images.

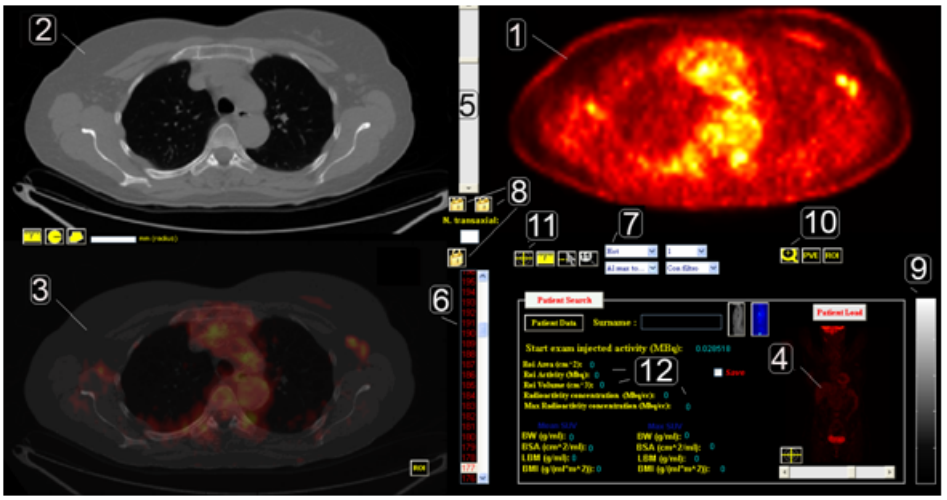

Figure A.1: Salient user interface elements of cOuch: 1)transaxial PET image 2)co-registrated CT transaxial image 3)PET/CT fused image 4)PET coronal image 5)slice control slider 6)slice number selection 7)pre-defined colorbar selection button 8)activation colorbar button 9)colorbar 10)zoom botton 11)pixel position and pixel value button 12)statistics ROI box.

Patient information are required by the software for store (see Figure A.2). If it has been entered by the technicians during the acquisition, these information are directly extracted from the image header file and stored in a file. Otherwise, some of the information can be manually entered. Parameters are required for PET/CT image quantification purposes.

In order to import data, the user is presented with a blank study and can import the medical images into the program: the image formats correctly detected are both DICOM and Analyze. After importing data, the entire study is saved in a proper directory and can be properly to interactively choose the image files.

The software allows contemporary visualization of each projection (transaxial, coronal and

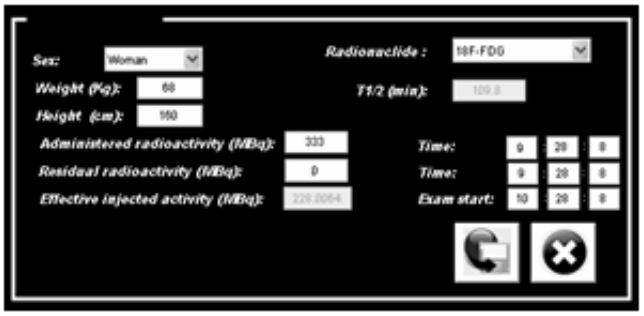

Figure A.2: Patient's data box. Height, weight, administered and residual activity and schedule of injection are obtained and saved by a proper form for analysis purposes. The effective injected activity corrected for the residual activity and reported to the exam start is automatically calculated.

sagittal projection) of both PET and CT images. A bicubic-spline function is applied to PET images as filter, providing smoothed images for visualization purposes, although original data are never altered for quantitative analysis. It is possible also to visualize PET images without smoothing in a proper window. The image dimensions are handled in terms of real world units (cm).

An automatic co-registration of PET and CT image modalities is performed by the cOuch software, obtaining a fused image by making PET image transparent by means of openGL rendering. Special care has to be taken for compensating for field of view differences between PET and CT images. A selection of pre-defined color tables can be chosen with the list selection to visualize both PET, CT and PET/CT fused images. A proper colorbar can be used to modify the current colormap dragging it with the touch/stylus to interactively alter the brightness and contrast of the image.

Graphical interface, including zoom/pan, utility bottoms, sliders, image selection buttons, are activated with manual touch or stylus input. When zoom is applied to a transaxial PET image, the other transaxial images are automatically resized. The slice control section allows to scroll through the images clicking over the images, or using the slider, or directly by entering a slice number. A proper tool allows to visualize pixel position and pixel value on PET image clicking over the PET image with the cursor.

ROIs can be defined on PET or CT or fused PET/CT transaxial images, using manual touch or stylus input along the desired trajectory and, in this way, optimising quantitative measurements. The drawn ROIs are replicated on each transaxial image. Different kinds of ROI, following the measurement techniques explained in chapter 2. All ROIs can be modified, translated on image using stylus dragging, once drawn, and saved, once fixed. For each fixed ROI the following values are calculated:

- Area
- Volume
- Activity
- ROI averaged radioactivity concentration
- Maximum radioactivity concentration

- Mean and maximum standardized uptake value normalized to body-weight (SUV_{BW}), lean body mass (SUV_{LBM}) and body surface area (SUV_{BSA})

The area of all ROIs is determined by the sum of the fractions of all pixels occupied by the ROIs.

Results of the quantitative analysis are automatically calculated and written to an Excel file for their loading and saving so as to be later opened for further analysis. This approach allows data files to be easily viewed and manipulated externally to the program.

A dedicated tool was developed to provide quantification of lesion radioactivity concentration on PET/CT images recovering underestimation due to PVE, following the RC-based developed method.: the operator has to draw a ROI on the lesion and a maximum of four ROIs on the background. The software evaluates the measured lesion-to-background ratio and the lesion dimension from the PET images or the CT images and performs automatically the correction using a proper Recovery Coefficient to compensate the loss of radioactivity concentration due to PVE. The corrected quantitative values are automatically calculated and saved on an Excel file.

An other software tool provides a collection of coronal/sagittal projections of PET-CT images with patient information that can be included in the PET image report and in witch annotations and text can be added for collaborative purposes. Then, physicians can write and compile patient text report using the stylus and the final report can be digitally signed, stored on PDF for archiving or email used or printed on film.

A proper tool allow to access to functions used to analyze and evaluate the correlations and of for data integration. A database was properly implemented in MySql in order to store all the parameters of interest for each patient. cOuch has been developed and installed, linked to the database for data statistical analysis. Several bi-variate and multivariate statistical tests (e.g. Wilcoxon-Mann-Whitney and Kruskal-Wallis correlation tests) have been implemented in cOuch to assay the relationship of quantitative PET parameters (e.g. SUV, functional lesion volume, anatomical lesion volume) with histological indexes (e.g. ER, PgR) and up/down regulated proteins (e.g.Adenosine kinase, Beta-actin). Moreover, a SUV-based dynamic threshold clustering algorithm was implemented to evaluate the correlation of SUV versus groups of parameters.

Bibliography

[1] LG. Strauss, D. Koczan, S. Klippel, L. Pan, C. Cheng, S. Willis, U. Haberkorn, and A. Dimitrakopoulou-Strauss. Impact of angiogenesis-related gene expression on the tracer kinetics of ^{18}F-FDG in colorectal tumors. *The Journal of Nuclear Medicine*, 49(8):1238–1244, Aug 2008.

[2] LG. Strauss, L. Pan, D. Koczan, S. Klippel, K. Mikolajczyk, C. Burger, U. Haberkorn, K. Schönleben, HJ. Thiesen, and A. Dimitrakopoulou-Strauss. Fusion of positron emission tomography (PET) and gene array data: a new approach for the correlative analysis of molecular biological and clinical data. *IEEE Transactions on medical imaging*, 26(6):804–812, Jun 2007.

[3] E. Segal, CB. Sirlin, C. Ooi, AS. Adler, J. Gollub, X. Chen, BK. Chan, GR. Matcuk, CT. Barry, HY. Chang, and MD. Kuo. Decoding global gene expression programs in liver cancer by noninvasive imaging. *Nature Biotechnology*, 25(6):675–680, Jun 2007.

[4] M. Soret, SL. Bacharach, and I. Buvat. Partial-volume effect in PET tumor imaging. *The Journal of Nuclear Medicine*, 48(6):932–945, Jun 2007.

[5] Available: http://www.spect.com/pub/*nema_iec_body_phantom_set*.pdf.

[6] LM. Graham, MM. Peterson and RM. Hayward. Comparison of simplified quantitative analyses of fdg uptake. *Nuclear Medicine and Biology*, 27(7):647–655, Oct 2000.

[7] P. Danna M. Giovacchini G. Landoni C. Picchio M. Gilardi MC. Savi A. Castiglioni I. Lecchi M. Bettinardi, V. Mancosu and F. Fazio. Two-dimensional vs three-dimensional imaging in whole body oncologic pet/ct: a discovery-ste phantom and patient study. *Quarterly Journal of Nuclear Medicine and Molecular Imaging*, 51(3):214–223, Sep 2007.

[8] H. Zaidi and KF. Koral. Scatter modelling and compensation in emission tomography. *European Journal of Nuclear Medicine and Molecular Imaging*, 31(5):761–782, May 2004.

[9] T. Antoch G. Freudenberg LS. Kühl H. Debatin JF. Bockisch, A. Beyer and Müller SP. Positron emission tomography/computed tomography–imaging protocols, artifacts, and pitfalls. *Molecular Imaging and Biology*, 6(4):188–199, Jul 2004.

[10] A. Matarrese M. Gianolli L. Sudati F. Pepe, A. Savi and MC. Gilardi. Performance characteristics of a bgo and a gso pet/ct scanner for the non-pure positron emitter ^{64}cu. *IFMBE Proceedings*, 25(2).

[11] EP. de Geus-Oei LF. Vriens, D. Visser and WJ. Oyen. Methodological considerations in quantification of oncological fdg pet studies. *European Journal of Nuclear Medicine and Molecular Imaging*, 37(7):1408–1425, Jul 2010.

[12] T. Tsujikawa, H. Otsuka, N. Morita, H. Saegusa, M. Kobayashi, H. Okazawa, and Nishitani H. Does partial volume corrected maximum SUV based on count recovery coefficient in 3D-PET/CT correlate with clinical aggressiveness of non-hodgkin's lymphoma? *Annals of Nuclear Medicine*, 22:23–30, Jul 2008.

[13] CF. Huang YJ. Konda SD. Appelbaum DE. Huang, YE. Chen and Y. Pu. Interobserver variability among measurements of the maximum and mean standardized uptake values on (18)f-fdg pet/ct and measurements of tumor size on diagnostic ct in patients with pulmonary tumors. *Acta Radiologica*, 51(7):782–788, Sep 2010.

[14] S. Moretti JL. Porcher R. Espié M. Lehmann-Che J. de Roquancourt A. Hamy AS. Cuvier C. Vercellino L. Groheux, D. Giacchetti and Hindié E. Correlation of high (18)f-fdg uptake to clinical, pathological and biological prognostic factors in breast cancer. *European Journal of Nuclear Medicine and Molecular Imaging*.

[15] R. Hoekstra OS. Twisk JW. Hoekstra CJ. Krak, NC. Boellaard and Lammertsma AA. Effects of roi definition and reconstruction method on quantitative outcome and applicability in a response monitoring trial. *European Journal of nuclear medicine*, 32(3):294–301, Mar 2005.

[16] NC. Hoekstra OS. Lammertsma AA. Boellaard, R. Krak. Effects of noise, image resolution, and roi definition on the accuracy of standard uptake values: a simulation study. *Journal of Nuclear Medicine*, 45(9):1519–1527, Sep 2004.

[17] BG. Bosmans G. van Kroonenburgh M. Stroobants S. Gregoire V. Lambin P. A. van Baardwijk, A. Baumert and Ruysscher D. The current status of fdg-pet in tumour volume definition in radiotherapy treatment planning. *Cancer Treatment Review*, 32(4):245–260, Jun 2006.

[18] A. Alavi A. Rousset, OG. Rahmim and H. Zaidi. Partial volume correction strategies in pet. *PET clinics*, 2(2):235–249, Apr 2007.

[19] JM. Prince JL. Bryan RN. McVeigh E. Leal JP. Davatzikos C. Müller-Gärtner, HW. Links and JJ. Frost. Measurement of radiotracer concentration in brain gray matter using positron emission tomography: Mri-based correction for partial volume effects. *Journal of Cerebral Blood Flow and Metabolism*, 12(4):571–583, Jul 1992.

[20] D. Strul and B. Bendriem. Robustness of anatomically guided pixel-by-pixel algorithms for partial volume effect correction in positron emission tomography. *Journal of Cerebral Blood Flow and Metabolism*, 19(5):547–549, Jul 1999.

[21] J. Van Laere K. Van Paesschen W. Ceyssens S. De Ceuninck L. Gheysens O. Kelles A. Van den Eynden J. Suetens P. Baete, K. Nuyts and P. Dupont. Evaluation of anatomy based reconstruction for partial volume correction in brain fdg-pet. *Neuroimage*, 23(1):305–317, Sep 2004.

[22] J. Bellemann ME. Trojan H. Haberkorn U. Schmidlin P. Brix, G. Doll and H. Ostertag. Use of scanner characteristics in iterative image reconstruction for high-resolution positron emission tomography studies of small animals. *European Journal of Nuclear Medicine*, 24(7):779–786, Jul 1997.

[23] PJ. Williams H. Hastings DL. Zweit J. Reader, AJ. Julyan. Em algorithm system modeling by image-space techniques for pet reconstruction. *IEEE Transaction on Nuclear Science*, 50(5):1392–1397, Oct 2003.

[24] FH. Hoekstra OS. Hoekstra CJ. Krak NC. Lammertsma AA. Hoetjes, NJ. van Velden and Boellaard R. Partial volume correction strategies for quantitative fdg pet in oncology. *European Journal of Nuclear Medicine*.

[25] SC. Hoffman, EJ. Huang and ME. Phelps. Quantitation in positron emission computer tomography:effect of object size. *Journal of Computer Assisted Tomography*, 3.

[26] RA. Pugsley JM. Li M. Kohlmyer SG. Vallires E.and Wood DE. Vesselle, H. Schmidt. Lung cancer proliferation correlates with [f-18]fluorodeoxyglucose uptake by positron emission tomography. *Clinical Cancer Research*, 6(10):3837–3844, Oct 2000.

[27] SI. Thödtmann R. Hanauske AR.and Schwaiger M. Weber, WA. Ziegler. Reproducibility of metabolic measurements in malignant tumors using fdg pet. *Journal of nuclear medicine*, 40(11):1771–1777, Nov 1999.

[28] X. Xing L. Mu D. Fu Z. Sun X. Sun X. Yang G. Zhang B. Sun X. Yu, J. Li and Ling CC. Comparison of tumor volumes as determined by pathologic examination and fdg-pet/ct images of non-small-cell lung cancer: A pilot study. *Int J Radiat Oncol Biol Phys*, 75(5):1468–1474, Dec 2009.

[29] O. Larson SM. Imbriaco M. Yeung H. Finn R. Erdi, YE. Mawlawi and JL. Humm. Segmentation of lung lesion volume by adaptive positron emission tomography image thresholding. *Cancer*, 80(12):2505–2509, Dec 1997.

[30] T. Basu S. Bural G. Surti S.and Alavi A. Srinivas, SM. Dhurairaj. A recovery coefficient method for partial volume correction of pet images. *Annals of nuclear medicine*, 23(4):341–348, Jun 2009.

[31] L. Eising EG. Heinze M. Brandau W. Jentzen, W. Freudenberg and Bockisch A. Segmentation of pet volumes by iterative image thresholding. *Journal of nuclear medicine*, 48(1):108–114, Jan 2007.

[32] JH. Schinagl, DA. Kaanders and WJ. Oyen. From anatomical to biological target volumes: the role of pet in radiation treatment planning. *Cancer Imaging*, 6.

[33] MA. Pratt BE. Hill C. Zweit J. McCready VR. Crawford, DC. Flower and CL. Harmer. Thyroid volume measurement in thyrotoxic patients: comparison between ultrasonography and iodine-124 positron emission tomography. *European Journal of nuclear medicine*, 24(12):1470–1478, Dec 1997.

[34] UE. Stumpe KDM. Hany TF.Bode B. Mende K. Veit-Haibach P. von Schulthess GK. Strobel, K. Exner and J. Hodler. The additional value of ct images interpretation in the differential diagnosis of benign vs. malignant primary bone lesions with ^{18}f-fdg-pet/ct. *European Journal of Nuclear Medicine and Molecular Imaging*, 35(11):2000–2008, Nov 2008.

[35] R. Boellaard. Standards for pet image acquisition and quantitative data analysis. *Journal of nuclear medicine*, 50(Suppl 1):11S–20S, May 2009.

[36] T. Nishiyama Y. Yamamoto Y. Ohkawa M. Hoshikawa, H. Mitani and N. Mori. Evaluation of the therapeutic effects and recurrence for head and neck cancer after chemoradiotherapy by fdg-pet. *Auris Nasus Larynx*, 36(2):192–198, Apr 2009.

[37] JM. Bacharach S. Graham MM. Karp J. Lammertsma AA. Larson S. Mankoff DA. Siegel BA. Van den Abbeele A. Yap J. Shankar, LK. Hoffman and D. Sullivan. Consensus recommendations for the use of ^{18}f-fdg pet as an indicator of therapeutic response in patients in national cancer institute trials. *Journal of Nuclear Medicine*, 46(6):901–903, Jun 2006.

[38] N. Avril, M. Menzel, J. Dose, M. Schelling, W. Weber, F. Jänicke, W. Nathrath, and M. Schwaiger. Glucose metabolism of breast cancer assessed by ^{18}F-FDG PET: histologic and immunohistochemical tissue analysis. *The Journal of Nuclear Medicine*, 42(1):9–16, Jan 2001.

[39] A. Gil-Rendo, F. Martínez-Regueira, G. Zornoza, MJ. García-Velloso, C. Beorlegui, and Rodriguez-Spiteri N. Association between ^{18}ffluorodeoxyglucose uptake and prognostic parameters in breast cancer. *British Journal of Surgery*, 96(2):166–170, Feb 2009.

[40] I. Hoekstra OS. Smit EF. Postmus PE. Teule GJJ. Lammertsma AA. Hoekstra, CJ. Paglianiti. Monitoring response to therapy in cancer using [f-18]-2-fluoro-2-deoxy-d-glucose and positron emission tomography: an overview of different analytical methods. *Eurpean Journal of Nuclear Medicine and Molecular Imaging*, 27(6):731–734, Jun 2000.

[41] R. Kumar, A. Chauhan, H. Zhuang, P. Chandra, M. Schnall, and A. Alavi. Standardized uptake values of normal breast tissue with 2-deoxy-2-[f-18]fluoro-d: -glucose positron emission tomography: variations with age, breast density, and menopausal status. *Molecular Imaging and Biology*, 8(6):355–362, Dec 2006.

[42] F. Warburg, O. Wind and E. Negelein. The metabolism of tumors in the body. *Journal of General Physiology*, 8(6):519–530, Mar 1927.

[43] C. Plathow and WA. Weber. Tumor cell metabolism imaging. *The Journal of Nuclear Medicine*, 49(6(Suppl)):43S–63S, Jun 2008.

[44] PR. Rich. The molecular machinery of keilin's respiratory chain. *Biochemical Society Transactions*, 31(6):1095–1105, Jun 2003.

[45] T. Johansson JJ. Williams JJ. Teräs, M. Tolvanen and J. Knuuti. Performance of the new generation of whole-body pet/ct scanners: Discovery ste and discovery vct. *European Journal of Nuclear Medicine and Molecular Imaging*, 34(10):1683–1692, Oct 2007.

[46] JS. Casey ME. DiFilippo FP. Hines H. Daube-Witherspoon, ME. Karp and G. Muehllehner. Pet performance measurements using the nema nu 2-2001 standard. *Journal of Nuclear Medicine*, 43(10):1398–1409, Oct 2002.

[47] PD. Guerrero TM. Digby WM. Hoffman, EJ. Cutler and JC. Mazziotta. Assessment of accuracy of pet utilizing a 3-d phantom to simulate the activity distribution of [18f]fluorodeoxyglucose uptake in the human brain. *Journal of Cerebral Blood Flow Metabolism*, 11(2):A17–A25, Mar 1991.

[48] P. Tylski, S. Stute, N. Grotus, K. Doyeux, S. Hapdey, I. Gardin, B. Vanderlinden, and I. Buvat. Comparative assessment of methods for estimating tumor volume and standardized uptake value in (18)F-FDG PET. *The Journal of Nuclear Medicine*, 51(2):173–175, Feb 2010.

[49] M. Bol A. Doumont T. Lonneux M. Daisne, JF. Sibomana and V. Grégoire. Tri-dimensional automatic segmentation of pet volumes based on measured source-to-background ratios: influence of reconstruction algorithms. *Radiotheraphy Oncology*, 69(3):247–250, Dec 2003.

[50] R. Cremerius U. Herholz K. Hoekstra O. Lammertsma AA. Pruim J. Young, H. Baum and P. Price. Measurement of clinical and subclinical tumour response using [18f]-fluorodeoxyglucose and positron emission tomography: review and 1999 eortc recommendations. *European Journal of Cancer*, 35.

[51] Y. Rousset, OG. Ma and Evans AC. Correction for partial volume effects in pet: principle and validation. *Journal of Nuclear Medicine*, 39.

[52] G. Panzacchi A. Gilardi MC. Castiglioni, I. Rizzo and F. Fazio. A mc-based pv correction method for pet/ct oncological studies. *IEEE-Nuclear Science Symposium and Medical Imaging Conference Record*.

[53] RT. Holden JE. Nickles RJ. Barbee, DL. Flynn and R. Jeraj. A method for partial volume correction of pet-imaged tumor heterogeneity using expectation maximization with a spatially varying point spread function. *Physics in medicine and biology*, 55(1):221–236, Jan 2010.

[54] H. Zaidi and I. El Naqa. Pet-guided delineation of radiation therapy treatment volumes: a survey of image segmentation techniques. *European Journal of Nuclear Medicine and Molecular Imaging*, 37(11):2165–2187, Nov 2010.

[55] CW. Elston and IO. Ellis. Pathological prognostic factors in breast cancer-i- the value of histological grade in breast cancer:experience from a large study with long follow-up. *Histopathology*, 19(5):403–410, Nov 1991.

[56] I. Di Rocco M. Leone BE. Garancini P. Mangili, F. Sassi and Santambrogio G. Breast carcinoma detection with a combination of radiolabeled monoclonal antibodies. promising results from immunohistochemistry studies. *Cancer*, 78(11):2334–2339, Dec 1996.

[57] DM. Schulz, C. Böllner, G. Thomas, M. Atkinson, I. Esposito, H. Höfler, and M. Aubele. Identification of differentially expressed proteins in triple-negative breast carcinomas using dige and mass spectrometry. *Journal of Proteome Research*, 8(7):3430–3438, Jul 2009.

[58] MC. Gast, JH. Schellens, and JH. Beijnen. Clinical proteomics in breast cancer: a review. *Breast Cancer Research and Treatment*, 116(1):17–29, Dec 2009.

[59] J. Kim, DH. Bae, JW. Lee, SY. Kim, YH. Kim, JY. Bae, JK. Yi, MH. Yu, DY. Noh, and C. Lee. Proteomic analysis of breast cancer tissue reveals upregulation of actin-remodeling proteins and its relevance to cancer invasiveness. *Proteomics. Clinical Application*, 3(1):30–40, Jan.

[60] F. Bertucci, D. Birnbaum, and A. Goncalves. Proteomics of breast cancer: principles and potential clinical applications. *Molecular and Cellular Proteomics*, 5(10):1772–1786, Oct 2006.

[61] L. Smith, MJ. Lind, KJ. Welham, and L. Cawkwell. Cancer proteomics and its application to discovery of therapy response markers in human cancer. *Cancer*, 107(2):232–241, Jul 2006.

[62] I. Pucci-Minafra, P. Cancemi, MR. Marabeti, NN. Albanese, G. Di Cara, P. Taormina, and A. Marrazzo. Proteomic profiling of 13 paired ductal infiltrating breast carcinomas abd bibtumoral adjacent counterparts. *Proteomics. Clinical Applications*, 1(1):118–129, Jan 2007.

[63] N. Avril, M. Schelling, J. Dose, WA. Weber, and M. Schwaiger. Utility of pet in breast cancer. *Clinical Positron Imaging*, 2(5):261–271, Oct 1999.

[64] N. Avril, S. Bense, SI. Ziegler, J. Dose, W. Weber, C. Laubenbacher, W. Römer, F. Jänicke, and M. Schwaiger. Breast imaging with fluorine-18-FDG PET: quantitative image analysis. *The Journal of Nuclear Medicine*, 38(8):1186–1191, Aug 1997.

[65] D. Vranjesevic, C. Schiepers, DH. Silverman, A. Quon, J. Villalpando, M. Dahlbom, ME. Phelps, and J. Czernin. Relationship between ^{18}F-FDG uptake and breast density in women with normal breast tissue. *The Journal of Nuclear Medicine*, 44(8):1238–1242, Aug 2003.

[66] AK. Buck, H. Schirrmeister, T. Mattfeldt, and SN. Reske. Biological characterisation of breast cancer by means of PET. *European Journal of Nuclear Medicine and Molecular Imaging*, 31(1(Suppl)):S80–S87, Jun 2004.

[67]

[68] M. Trassard M. Hacène K. Phillips E. Tubiana-Hulin M. Spyratos, F. Ferrero-Poüs and V. Le Doussal. Correlation between mib-1 and other proliferation markers. *Cancer*, 94(8):2151–2159, Apr 2002.

[69] DJ. Holloway P. Kay EW. McCann AH. Landberg G. Duffy MJ. Jirstrom K. Rexhepaj, E. Brennan and WM. Gallagher. Novel image analysis approach for quantifying expression of nuclear proteins assessed by immunohistochemistry: application to measurement of oestrogen and progesterone receptor levels in breast cancer. *Breast Cancer Research*, 10(5):R89, Oct 2008.

[70] E. Greene GL. Konrath J. Leight GS. Kinsel, LB. Szabo and KS. Jr. McCarty. Immunocytochemical analysis of estrogen receptors as a predictor of prognosis in breast cancer patients: Comparison with quantitative biochemical methods. *Cancer Research*, 49(4):1052–1056, Feb 1989.

[71] Tavassoli FA and Devilee P. *World Health Organization Classification of Tumours: Pathology and Genetics of tumours of the Breast and Female Genital Organs*. IARC Press, 2003.

[72] AJCC. *7th Edition AJCC Cancer Staging Manual*. Springer, 2010.

[73] L. Sgro L. Mininanni P. Moggio G. Biglia, N. Mariani and P. Sismondi. Increased incidence of lobular breast cancer in women treated with hormone replacement therapy: implications for diagnosis, surgical and medical treatment. *Endocrine-Related Cancer*, 14(3):549–567, Sep 2007.

[74] LN. Trefethen and D. Bau. *Numerical Linear Algebra*. Society for Industrial and Applied Mathematics, 1997.

[75] A. Gilardi M.C. Messa C. Canevari C. Gallivanone, F. Stefano and I. Castiglioni. Partial volume correction methods based on measured lesion-to-background ratio in pet-ct oncological studies. *IFMBE Proceedings 25/II*.

Ringraziamenti

Un doveroso ringraziamento alla Prof.ssa Maria Carla Gilardi e alla Prof.ssa Cristina Messa per avermi dato la possibilità di portare avanti un progetto di ricerca interessante e stimolante, lavorando in un ambiente dinamico e ricco.

Un grande ringraziamento alla Dott.ssa Isabella Castiglioni per avermi seguito con pazienza in questi tre anni, per essersi presa cura di me e per avermi dato la possibilità di esprimere le mie capacità.

Grazie alla Prof.ssa Galli, per l'attenzione che ha dedicato affinchè la Scuola di Dottorato diventasse di qualità, anche a costo di scelte che non sempre piacciono ai dottorandi.

Grazie alla Prof.ssa Del Puppo che si occupa in modo sempre materno di studenti e dottorandi, prodigandosi in lungo e in largo per loro.

Grazie ad Eugenio: senza di te questi anni di dottorato sarebbero stati decisamente meno intellettualmente stimolanti e meno lavorativamente fruttosi.

Grazie ad Annalisa: per aver condiviso con cuore tanti momenti di lavoro belli e brutti.

Grazie ad Alessandro: abbiamo cominciato questo percorso assieme ed è sempre bello potersi confrontare ed aiutare.

Grazie ad Eleonora per la semplicità con cui mi ha aiutata a vivere alcune situazioni in ospedale.

Grazie a Carla per avermi sempre regalato allegria e disponibilità sia nel lavoro sia nell'amicizia.

Grazie a Simone, per l'affettuosa amicizia che mi regala e perchè senza il suo pc, non so come avrei potuto scrivere la tesi!

Grazie a mio marito Thomas: già sai quanto mi sei caro, ma, visto che le cose vanno dette, grazie perchè non mi permetti mai di scoraggiarmi e perchè se non mi avessi aiutato con il patatino, sacrificando anche alcuni tuoi momenti liberi, ci avrei impiegato il doppio del tempo a scrivere la metà di questa tesi.

Grazie a babbo Marco e mamma Marina: siete insostituibili in ogni passo della mia vita e vi voglio bene!

Grazie Vale perchè abbiamo "sudato" e ottenuto una comunione di anime che è quasi introvabile: spero di poterti regalare quello che mi stai donando tu.

Grazie Sammy: quando diventerai grande, ti racconterò che non è stato facile rimanere incinta durante il dottorato, che non è stato facile partorire, che non è stato facile lasciarti a casa così piccolo per tornare al lavoro, ma ti dirò anche che sei stato la cosa più bella che ho fatto e che non dimenticherò mai la gioia che ho provato nel tenerti tra le mie braccia (spero che mi permetterai di farlo ancora a lungo!).